Assessing sensitivity regimes of secondary inorganic aerosol formation in Europe with the CALIOPE-EU modeling system

María T. Pay[a], Pedro Jiménez-Guerrero[b], José M. Baldasano[a,c]

[a]Earth Sciences Department, Barcelona Supercomputing Center-Centro Nacional de Supercomputación, Barcelona, Spain.

[b]Physics of the Earth, University of Murcia, Spain.

[c]Environmental Modeling Laboratory, Technical University of Catalonia, Barcelona, Spain.

*Corresponding author: jose.baldasano@bsc.es. Earth Science Department, Barcelona Supercomputing Center-Centro Nacional de Supercomputación (BSC-CNS). Jordi Girona 29, Edificio Nexus II, 08034 Barcelona, Spain. Tel.: +34 93 413 77 19; Fax: +34 93 413 77 21

Abstract

Modeling and measuring studies have shown that sulfur dioxide and nitrogen oxides form two of the chemical component with the largest contribution to PM2.5 in Europe: ammonium sulfate and ammonium nitrate. Site-specific observations can more accurately characterize the distribution of pollutant, but cannot predict the effectiveness of emission control. Understanding (and controlling) the formation regimes for these components can importantly contribute to the achievement of the reduction objectives established in the European legislation for PM2.5 (20% of PM2.5 triennial for mean of urban background levels between 2018 and 2020). In this sense, the CALIOPE-EU high-resolution air quality modeling system (12 km x 12 km, 1h) has been implemented in this work in order to investigate the formation of secondary inorganic aerosols (SIA) (SO_4^{2-}, NO_3^- and NH_4^+, which involve an important part of particulate matter over Europe) with respect to gas-phase precursor concentrations (SO_2, HNO_3 and NH_3) during the year 2004. The modeling system performs well at estimating inorganic species when compared to the measurements of EMEP monitoring network, but errors are larger for precursor species. Ammonia is underestimated in warmest months, nitric acid tends to be overestimated in the summer months, and sulfur dioxide appears to be systematically overestimated. The temporal treatment of ammonia emission is found to be source of uncertainty in the model representation of SIA. Furthermore, we discuss the annual pattern for each inorganic aerosol and gas precursor species over Europe estimated with the EMEP data and CALIOPE-EU outputs, comparing the performance with other European studies. In order to understand the sensitivity of each SIA component to the emission their precursors, the spatial distribution of several widely-used indicators is also

included. Results indicate that sulfate ion is not usually fully neutralized to ammonium sulfate in ambient measurements and is usually fully neutralized in model estimates. CALIOPE-EU and EMEP concentrations agree that the more continental regions in Europe tend to be HNO_3-limited for nitrate formation. Regulatory strategies in this region should focus on reductions in NO_x rather than NH_3 to control ammonium nitrate. CALIOPE-EU provides us an opportunity to assess how well the modeling system reproduces the spatial and temporal variability of important precursor species and co-located ions and also complement the measurement findings.

Keywords: Air quality, model evaluation, aerosol precursors, geochemistry, sulfate, nitrate, ammonia

1 Introduction

Atmospheric particulate matter (PM), or aerosols, play a central role in atmospheric processes (Fountoukis and Nenes, 2007). They have adverse effects on human health (Pope et al., 2009) and affect visibility (Altshüller, 1984), ecosystems (Niyogi et al., 2004; Bytnerowicz et al., 2007), air quality and climate change (IPCC, 2007). To alleviate some of these atmospheric problems, the control atmospheric PM concentration is demanding. European legislation has established regulations regarding PM10 (particles with $d_p < 10$ μm) and recently for PM2.5 ($d_p < 2.5$ μm) in order to reduce human exposure to high concentration of PM (European Commission, 2008).

PM is both emitted directly from a large variety of anthropogenic, biogenic and natural sources and formed in the atmosphere by chemical and physical processes from gas-phase precursors such as NMVOC, NO_x ($NO+NO_2$), SO_2 and NH_3 (Seinfeld and Pandis, 1998). Therefore, to fulfill the task of reducing human exposure to PM, policies must focus not only on the reduction of primary particulate emissions, but also on the reduction of precursor emissions for the formation of secondary particles (Wu et al., 2008; Renner and Wolke, 2010).

Several experimental studies have analyzed levels, speciation and origin of PM over Europe (Querol et al., 2004, 2009; van Dingenen et al. (2004); Putaud et al., 2004, 2010). They found that the European background levels, derived form 31 European air monitoring stations, have been 7.0±4.1 μgPM10 m^{-3} and 4.8±2.4 μgPM2.5 m^{-3}, over the past decade. The observed

aerosol composition reveled that organic matter is the major component in PM10 and PM2.5, except at rural background sites where secondary inorganic aerosol (SIA) contribution prevailed. The dominant SIA species are ammonium sulfates ($(NH_4)_2SO_4$) and ammonium nitrates (NH_4NO_3) salts.

The formation of SIA is a two-step process. First, the primary emissions of NO_x and SO_2 are oxidized to form aerosol precursor nitric acid (HNO_3) and sulfuric acid (H_2SO_4), respectively, precursors of secondary aerosols. Second, a fraction of the H_2SO_4, HNO_3 and NH_3 partition between the gas and particle phase according to thermodynamic equilibrium determined by temperature, relatively humidity and molar concentration of SO_4^{2-}, total nitrate (TNO_3=HNO_3+ NO_3^-) and total ammonia (TNH_3=NH_3+ NH_4^+). SO_2 emissions in Europe have been reduced ~67% from 1980 to 2000 (EMEP, 2004; Fagerli and Aas, 2008; Hamed et al., 2010). Thus, nowadays less NH_3 is converted to $(NH_4)_2SO_4$ and more NH_3 is available for the formation of NH_4NO_3. This situation leads to a higher residence time of TNO_3 in air (Fagerli and Aas, 2008).

Because of the complex relationship between SIA (Ansari and Pandis, 1998; Vayenas et al, 2005) the control of PM2.5 is still nowadays a difficult challenge. In this sense, air quality models (AQMs) are important tools for air quality management and the evaluation of emission control policies, but it becomes necessary to assess their ability not only in simulating air quality levels, but also to perform diagnostic evaluations. Single model evaluation studies (Schaap et al., 2004a, Sartelet et al., 2007; Stern et al., 2008; Matthias, 2008), model inter-comparision (Hass et al., 2003, van Loon et al., 2004); and model ensembles (Vautard et al., 2009) showed that models tend to underestimate observed PM. Furthermore, Renner and Wolke (2010) modeled the formation of atmospheric transport of SIA over high ammonia emissions areas in north Germany. The results of these studies point to large uncertainties in the estimation of the meteorological input data; uncertainties in the modeling of the anthropogenic PM sources, missing natural and anthropogenic sources and also with gaps in the knowledge of many of the physical and chemical processes which lead to the formation of SIA.

So, the main objective of this work is to investigate the formation regimes of SIA over Europe by means of the CALIOPE-EU air quality modeling system (Pay et al., 2010a; Baldasano et al., 2011) with a simulation covering the whole year 2004. For that purpose, this paper is structured as follows. Section 2 describes the modeling system, the observational database

and the evaluation tools. Section 3 analyses the modeling results against available measured data for the year 2004 and discusses the modeled and observed annual patterns of SIA and their gas-precursors. Also a discussion about aerosol formation regimes over Europe is provided. Section 4 presents a thorough comparison with other European studies. Finally, conclusions are drawn in Section 5.

2 Methods

2.1 CALIOPE-EU modeling system

CALIOPE (Baldasano et al., 2008a) is a complex system that integrates a meteorological model (WRF-ARW), an emission processing model (HERMES-EMEP), a chemical transport model (CMAQ) and a mineral dust dynamic model (BSC-DREAM8b) together coupled in an air quality modeling system (Fig. 1 of Pay et al., 2010a). CALIOPE encompasses a high-resolution air quality modeling system which provides 48-h air quality forecasts in Europe (12 km x 12 km) and Spain (4 km x 4 km) (available at: www.bsc.es/caliope). The system has been widely evaluated during its development over northeastern Spain (Jiménez et al., 2005a,b, 2006a,b, 2007), the Iberian Peninsula (Jiménez-Guerrero et al., 2008a; Baldasano et al., 2008a, 2011; Pay et al., 2010b) and Europe (Pay et al., 2010a). Furthermore, it has been used for assessing air pollution dynamics (Gonçalves et al., 2009a) and as management tool to study air quality impact of urban management strategies (Jiménez-Guerrero et al., 2008b; Golçalves et al., 2008; 2009b; Soret et al., 2011).

CALIOPE system applied over the European domain in 2004 is namely thereinafter as CALIOPE-EU. For a detailed description of the modeling system we refer to aforementioned studies. Here, we summary the main characteristics for this study.

Meteorological input data for the photochemical modeling runs are processed using the Advanced Research Weather and Forecasting model (WRF-ARW) version 3.6.1 (Michalakes et al., 2004; Skamarock and Klemp, 2008).

The Models-3 Community Multiscale Air Quality Modeling System (Models-3/CMAQ) version 4.5 is a three-dimensional Eulerian photochemical transport model that uses state-of-the-science routines to model gas and particulate matter formation and removal processes (Byun and Schere, 2006; Appel et al., 2008; Roy et al., 2007). The model is applied with the Carbon Bond IV chemical mechanism (CBM-IV, Gery et al., 1989) following the criteria of

Jiménez et al. (2003). Photolysis rates are computed off-line, as done in the photolysis rate preprocessor JPROC. The aerosols are modeled using the AERO4 module (Binkowski and Roselle, 2003) which comprises the following aerosol components: NO_3^-, SO_4^{2-}, NH_4^+, elemental and organic carbon. SIA are generated by nucleation processes from their precursors. Then, the ISORROPIA thermodynamic module (Nenes et al., 1998) computes the equilibrium between gaseous HNO_3, NH_3 and fine-particle NO_3^-, SO_4^{2-}, NH_4^+, and aerosol water.

Emission data are processed using the High-Elective Resolution Modeling Emission System (HERMES, Baldasano et al., 2008). In the European domain, the inventory of the anthropogenic emissions of SO_2, NO_x, NMVOC, CO, PM, and NH_3 is derived from the 2004 annual EMEP emission database (EMEP, 2007). The inventory uses the source categories following the Selected Nomenclature Air Pollution (SNAP). Disaggregation of EMEP (50 km x 50 km) data is performed in space (12 km x 12 km) and time (1h). The spatial and temporal top-down disaggregation is sector-dependent. In the horizontal dimension, emission data are remapping to finer grid applying different criteria through three datasets (1) high-resolution land use map (EEA, 2000), (2) coordinates of industrial sites (EPER), and (3) vectorized road cartography of Europe (ESRI). In the vertical dimension, the sector-dependent emission distribution for gases is applied following the EMEP model (Simpson et al., 2003). In the time dimension, data are mapping from annual to an hourly basis using the temporal factors of EMEP/MSC-W (Meteorological Synthesizing Centre-West). Biogenic emissions are estimated internally as a function of temperature, radiation and land-use (Baldasano et al., 2008).

Fig. 1 and Table 1 show the annual averaged emissions of the most contributed sectors of the emitted compounds SO_x, NO_x, NH_3 and NMVOC in Europe. In 2004, 56% of the total SO_x emissions were attributed to energy transformation. 64% of NO_x total emissions are attributed to transport (road and no-road, sector 7 and 8). 94% of NH_3 total emissions are attributed to agriculture and livestock. Domestic animals contribute most to total emissions, followed by fertilizers, crops and others. The fact that agricultural activities contribute most to ammonia emissions implies that densely populated regions tend to have the highest ammonia emissions. 33% of VOC total emissions are attributed to on-road transport and other 33% to the use of solvents. Last, 50% of CO total emissions are attributed to on-road transport.

The photochemical modeling domain consists of 479 cells in the X direction and 399 cells in the Y direction covering the European domain with 12 km x 12 km grid cells in a Lambert projection. The CMAQ horizontal grid resolution corresponds to that of WRF. Its vertical structure was obtained by a collapse from the 38σ-WRF layers to a total of 15 σ-layers steadily increasing from the surface up to 50 hPa with a stronger concentration within the PBL. The chemical boundary conditions are based on the global climate chemistry model LMDz-INCA2 (Piot et al., 2008; Szopa et al., 2009).

2.2 Air quality network for gas and aerosol phase

Model output for gas precursors and SIA particulate phase concentrations are compared with ground-based measurements of SO_2, SO_4^{2-}, HNO_3, NO_3^-, NH_3, NH_4^+, TNO_3, and TNH_3 from the EMEP monitoring network for the year 2004. EMEP stations are assumed to be representative of regional background concentrations (Torseth and Hov, 2003). Therefore, the authors wish to stress that the model performances presented in this paper are evaluated only for background concentrations. EMEP has an extensive quality control of the data that are included in the database, freely available on its web page (http://www.emep.int). However, accurate measurements of SIA aerosol remain a challenge. Inorganic species may be accurately measured with an uncertainty of about ±10% for major species (Putaud et al., 2004). Hence, measured NO_3^- and NH_4^+ are found to be uncertain under warm conditions (Schaap et al., 2004b).

All EMEP measurement data are given on a daily average. As a result, 31 stations were selected to evaluate SO_2, 53 for SO_4^{2-}, 8 for HNO_3, 31 for NO_3^-, 7 for NH_3, and 15 NH_4^+, for respectively. SIA and gas precursors are also indirectly evaluated with measurements of TNO_3 and TNH_3 available over 31 stations. The selected EMEP stations and measured pollutants that are used for this comparison are briefly described in Table 2 and presented in Fig. 2. Note that the final coverage of the dataset is rather disperse since France, Italy and southeastern Europe only include several stations. Also, it is important to remark that the availability of stations measuring nitrogenous gas precursors (HNO_3 and NH_3) is scarce and not well distributed.

2.3 Evaluation and assessment tools

Modeled aerosol outputs are post-processed for the comparison with quantified measured. A list of CMAQ aerosol module variables can be found in Table 1 of Binkowski and Roselle

(2003). From these variables, fine-particles SO_4^{2-}, NO_3^-, and NH_4^+ are approximated by summing the appropriate Aitken- and accumulation-mode concentrations. Although CALIOPE-EU system estimates sulfate from sea salt, fine-particle sulfate only takes into account that with anthropogenic origin, hereinafter referred to as SO_4^{2-}.

To pair observations and model results in space a bilinear interpolation is used, since EMEP are representative of regional background concentrations. Measurements are in daily basis, thus aerosols are compared in terms of daily averages from the modeling system.

Metrics used to describe the modeling system performance include classical statistics. Besides mean of modeled and measured values we show mean bias (MB), root mean square error (RMSE), correlation coefficient (r), mean fractional bias (MFB), and error (MFE) (Boylan and Russell, 2006; Dennis et al., 2010). The bias and error describe the performance in terms of the measured concentration units ($\mu g\ m^{-3}$) assuming that measurements are the truth. On the other hand, fractional metrics describe performance as a percent, taking into account that the measurements have their own uncertainty due to biases and artifacts related to sampling and laboratory analysis methods (Boylan and Russell, 2006; Putaud et al., 2010). The best model performance is when MFB and MFE approach 0. The fractional metrics are bounded by 200%, which is considered very poor performance. The fractional bias and error metrics normalize large and small concentrations, making seasonal trends in model performance more discernable.

The aerosol compounds are compared to the daily averages from the model, and daily statistics and graphics methods were computed to describe the model skills and weaknesses. The inorganic and organic chemical species data were analyzed from the PM2.5 fraction, whereas natural aerosol such as sea spray and mineral dust from the Saharan desert, were analyzed from the PM10 particle concentrations.

The bias metrics between SIA and gas-phase precursors are examined for relationships to determined how much of the error in precursor model performance translates into error for co-located ion model estimates. Besides, to assess the chemical behavior of aerosol chemical composition, we introduce four indicators extracted from bibliography to examine the SIA formation regimens. S-ratio (Hass et al., 2003) indicates the ability of the model to form the sulfate aerosols. Concentrations are expressed as $\mu g\ m^{-3}$ in the S-ratio equation.

$$S-ratio=\frac{SO_2}{SO_2+SO_4^{2-}}$$

SO_4^{2-} is produced during the transport by heterogeneous processes in clouds. A ratio close to unity indicates that only a small fraction of the emitted SO_2 has been converted to the sulfate aerosol.

Free ammonia ($F\text{-}NH_x$) indicator quantifies the amount of ammonia available, after neutralizing SO_4^{2-}, for NH_4NO_3 formation. This indicator is based on the fact that $(NH_4)_2SO_4$ aerosol is the favored form for sulfate. $F\text{-}HH_x$ is defined as the total ammonia minus twice the sulfate concentration on a molar basis:

$$F-NH_x=TNH_3-2SO_4^{2-}$$

The gas-aerosol equilibrium in the $SO_4^{2-}/NO_3^-/NH_4^+$ system is analyzed using the G-ratio (Ansari and Pandis, 1998; Pinder et al., 2008) which indicates whether fine-particle NO_3^- formation is limited by the availability of HNO_3 or NH_3. All the terms in the following equation are expressed molar basis (μmole m^{-3}).

$$G-ratio=\frac{F-NH_x}{TNO_3}$$

G-ratio > 1 indicates that nitric acid is limiting, while G-ratio < 0 indicates the ammonia is severely limiting. G-ratio between 0 and 1 indicates ammonia is available for reaction with nitric acid, but ammonia is the limiting species.

Pinder et al. (2008) suggested an adjust G-ratio which takes into account that sulfate is not always fully neutralized. That is true especially during winter, when nitrate is thermodynamically more stable than sulfate. However, we decided not to use this adjust G-ratio since only 5 stations are available to evaluate the modeled pattern.

3 Results and discussion

First, in Section 3.1, a model evaluation is performed through statistical performance. Fig. 3 compares the CALIOPE-EU model outputs with measurements for inorganic aerosols (sulfate, nitrate and ammonium) and their precursors (sulfur dioxide, nitric acid and ammonia) computed on a daily basis using all the EMEP stations with available data. Also, Fig. 4 shows

the monthly MFB and MFE for each species (gas and precursor) compared to proposed performance goals and criteria by Boylan and Russell (2006). Second, in Section 3.2, a general description of the annual mean distribution of each pollutant is provided to determine each pattern across Europe (Fig. 5). Latter, Section 3.3 the discussion is focused on the use of indicators that allow detecting SIA formation regimens over Europe (Fig. 6).

3.1 Model evaluation

3.1.1 Sulfur dioxide and sulfate

For SO_2, the model results are evaluated against 31 stations located across the Iberian Peninsula, central and north-eastern Europe. Fig. 3a for SO_2 shows the temporal evolution of CALIOPE-EU system which is able to reproduce the annual variation of daily measurements ($r = 0.60$) although it overestimates some observed peaks (MB = 0.5 $\mu g\ m^{-3}$). As shown in Fig. 4a and b bias and errors for SO_2 do not present a significant seasonal variation. Monthly biases are relatively low (0 % < MFB < 30 %) and fall within the performance goal proposed by Bolan and Russell (2006). Nevertheless monthly fractional errors only accomplish the criteria (60 % < MFE < 75 %).

SO_4^{2-} concentrations are compared with 53 stations which cover Spain, eastern and central Europe and Nordic countries. The annual variability of the modeled SO_4^{2-} concentrations agrees fairly well with measurements ($r = 0.49$, RMSE = 1.3 μgm^{-3}) and modeling results present a low negative bias along the year (MB < -0.3 μgm^{-3}) (Fig. 3b). Best model performances are achieved during warm seasons (MFB ~ 0% and MFE ~50 %, Fig. 4a and b) when ambient concentrations are highest due to enhanced photochemistry, low air mass renovation regional scale, and the increase of the summer mixing layer depth favoring the regional mixing of polluted air masses (Querol et al., 2009). Only during cold seasons SO_4^{2-} from CALIOPE-EU does not accomplish the goal for MFB and MFE. This result is geographically biased by winter underestimations at eastern European stations (E. Eu region), where MB by station ranges from -0.5 $\mu g\ m^{-3}$ to -2.5 $\mu g\ m^{-3}$.

January and March undergo three major episodes of enhanced SO_2 and SO_4^{2-}. The model reproduces accurately the SO_2 variability meanwhile sulfate events are not reproduced. Overall, the positive mean bias only for SO_2 suggests that non-marine SO_4^{2-} formation in the modeling system is often limited by oxidant availability and not always by sulfur dioxide availability. Winter underestimation of SO_4^{2-} is a common issue in most models integrated in

Europe which represent a direct couplet of sulfur chemistry with photochemistry, even detected with CMAQ over Europe (Matthias, 2008). This feature can be probably explained by a lack of model calculated oxidants or missing reactions (Kasibhatla et al., 1997). In this context, besides the gas phase reaction of SO_2 by OH, Tarrasón and Iversen (1998) and Schaap et al. (2004a) included additional oxidation pathways in clouds under cool and humid conditions that improve modeled SO_4^2 performance.

3.1.2 Nitric acid, nitrate and total nitrate

HNO_3 is evaluated over 8 EMEP stations located in eastern Europe, Nordic countries and Italy. Overall, CALIOPE-EU system is able to reproduce annual variability for HNO_3 (Fig. 3c), presenting the highest values during summer as measurements (r = 0.41, RMSE = 1.1 μgm^{-3}). However, as shown also in Fig 4c and d, CALIOPE-EU underestimates HNO_3 in coldest months (MFB > -30%), has a small bias during spring (MFB≤±30%, within the goals) and overestimates in summer seasons (MFB > 30%). CALIOPE-EU NO_2 concentrations have already been evaluated over EMEP in Pay et al. (2010a). The MFB for NO_2 was examined by season and did not show a strong seasonal trend, but the lowest bias are found in summer and spring (MFB ~ -50%). This finding, together with an overestimation of HNO_3 in warm seasons indicates that either the chemical transport model (CMAQv4.5) may be generating too much nitric acid though photochemical reactions or summer deposition processes are not appropriately characterized (Baker and Scheff, 2007).

The NO_3^- concentrations are evaluated over 31 EMEP stations which cover mainly Spain and central Europe. Time series in Fig. 3d show that the modeling system reproduces the NO_3^- daily variability throughout the year (r=0.58, RMSE= 2.3 $\mu g\ m^{-3}$), presenting higher levels during winter and lower levels during summer due to its thermal instability (Querol et al., 2009). NO_3^- concentrations are on average underestimated, although large underestimations and errors are found in warm seasons (Fig. 4c and d) with |MFE| ~ 130%. Note that summer underestimation occurs under low concentrations where relative model performance is not as important; indeed, both the model and observed NO_3^- are typically quite low during summertime (Fig. 3c). In any case, monthly fractional biases and errors for NO_3^- fall within the criteria. The NO_3^- errors are roughly 2 times higher than the corresponding SO_4^{-2} errors, reaching till 3 times in summer. Such finding is consistent with other modeling studies (Yu et al., 2005; Tesche et al., 2006). Diagnostic evaluations performed by Yu et al. (2005) indicate

that a large source of error in simulating nitrate came from errors in the simulation of total ammonia, sulfate and, to lesser extent, total nitrate.

Measurements of TNO_3 are available over 31 stations covering Spain, north and central Europe. The TNO_3 in the modeling system reproduces the annual trend with high temporal correlation as shown the temporal series in Fig. 3g (r = 0.50, RMSE = 1.1 µg m^{-3}). High modeled and measured levels of TNO_3 in winter can be explained by the higher stability of NH_4NO_3 in winter, which causes a higher portion of the NO_3^- to partition to aerosol, which has a longer lifetime than nitric acid against deposition (Schaap et al., 2004a). Monthly fractional biases and errors (Fig. 4c and d) indicate that large deviations are presented in the coldest months, dominated by the calculated underestimation of HNO_3 and NO_3^- in these seasons (MFB < -50%). The low fractional bias in summer results from the compensation error between the overestimation of HNO_3 (MFB ~ 50%) and underestimation of NO_3^- (MFB ~ -130%). In warm months (from April to October) the model fractional biases and error are within the criteria: MFB≤±60 and MFE ≤75.

The largest underestimations are located over the E.IP-W.Med and C.Med regions and the Eastern Europe (E.Eu regions, except Illmitz and Sniezka) with mean biases of -1.8 µg m^{-3} and -1.5 µg m^{-3}, respectively in both areas. The model presents the best skills in the western Iberian Peninsula, with high correlations ranging from 0.40 to 0.65 by stations, and with annual mean biases less than 1.0 µg m^{-3}, and RMSE less than 1.3 µg m^{-3}.

3.1.3 Ammonia, ammonium and total ammonia

NH_3 is measured in 7 stations located in western Iberian Peninsula (2), central Mediterranean (1), and northern (2) and eastern (2) Europe. Temporal series (Fig. 3e) indicate that the CALIOPE-EU system reproduces the annual variability for NH_3 (r = 0.56) with a low mean bias (MB = -0.4 µg m^{-3}). However, during warm season, April to August, modeled NH_3 is systematically underestimated. NH_3 emissions predominantly come from agricultural sources, primarily from livestock animal waste (Table 1). Livestock sources vary during the year since volatilization of NH_3 from the animal waste is a function of temperature (Gilliland et al, 2003). Seasonality in NH_3 emission is expected since field application of fertilizers occurs during specific seasons (Asman, 2001).

A total of 15 EMEP stations provide measurements of NH_4^+ to evaluate ammonium in 2004, mainly covering eastern Europe. Modeled NH_4^+ comparisons to measured data (Fig. 3f) revels

that annual variability is correctly reproduced (r = 0.62, RMSE= 1.2 µg m^{-3}). However annual mean model is on average underestimated in 36%. Monthly fractional errors (Fig. 4e and f) fall within the criteria (-60% < MFB < 0 and MFE < 75%) except in the coldest months. Despite the underestimations during winter, the temporal variability is correctly captured in these months (r = 0.70).

TNH_3 measurements are available over 31 stations covering Spain, north and central Europe. The temporal series (Fig. 3f) indicates that the TNH_3 levels are on average in agreement with observation along the year (r = 0.50, RMSE = 2.1 µg m^{-3}) with relatively low bias (MB = - 0.5 µg m^{-3}). The fractional bias distribution by months (Fig.4 e and f) for TNH_3 shows that the modeling system does not provided enough TNH_3 in spring (MFB ~ -25%) and lightly too much in winter (MFB ~ 10%). TNH_3 falls within criteria for fractional bias and error, but partition between gas and aerosol is not totally well characterized. On one hand, TNH_3 underestimation in the warm season is biased by gas-phase NH_3 which presents its largest underestimation from May to August with MFF ~ -100% (Fig. 3e). On the other hand, TNH_3 overestimations in winter are biased by the tendency of the model to overestimate gas-phase NH_3 at some stations (Fig. 3e).

From May to October, SO_4^{2-} is overestimated (MFB ~10%) and NH_4^+ reaches its minimum bias (MFB ~ - 10%). In this case, the underestimation of ammonia during the same period indicates that the excessive SO_4^{2-} in the model keeps ammonium in the particulate phase when it should be in the gas phase or available to potentially neutralize NO_3^-. This fact also explains the maximum overestimation of HNO_3 (MFB ~ 50%), the large underestimation of NO_3^- (MFB ~ -120%) and the minimum bias in TNO_3 (MFB ~ -20%) during the same period, since too much NO_3^- is remaining in the gas phase because there is not enough NH_4^+ to neutralized NO_3^-. This fact demonstrates that temporal representation of NH_3 emission could have a large effect on the results. Significant uncertainty exists in the magnitude and temporal variability of NH_3 emissions in Europe (Gilliland et al., 2003; Schaap et al. 2004a; Gilliland et al., 2006).

3.1.4 Bias relationship between SIA and gas precursors

The relationship in model-observation bias for SIA species and precursors is examined using the correlation coefficient (Table 3) to determine whether biases in precursor species directly translates into biases for aerosol species. These correlation coefficients compare the bias metric distributions over all sites and days for a pair of species. A number close to 1 indicates a strong relationship in the bias metric between a pair of species. A strong relationship is seen

between model-observation bias for SO_4^{2-} and NH_4^+ (bias correlation = 0.59) and also between NO_3^- and NH_4^+ (bias correlation = 0.75). This makes sense since these ions are chemically coupled in the atmosphere. SO_2 bias has a fairly weak relationship with SO_4^{2-} bias, which is interesting since a more direct relationship might be expected between them. HNO_3 and NH_3 bias is weakly associated with biases in the aerosol species (bias correlation < 0.1). These weak relationships between precursor gases and aerosol species indicate that model performance for precursor gases does not directly translate into model biases for particulate matter species in the same ambient sample. This likely reflects the different time scales of particulate formation and the influence of the regional transport.

3.2 Pattern description

Next section discusses the spatial distribution of annual concentrations modeled with CALIOPE-EU system (12 km x 12 km) for SIA and gas-phase precursors in 2004 taking into account annual mean concentrations measured with EMEP monitoring network.

3.2.1 Sulfur dioxide and sulfate

Fig. 5a shows the SO_2 pattern over Europe which presents a significant relationship with the distribution of SO_2 emission sources in Fig. 1c. They are mainly produced by power generated and transformation industries (Table 1) located in northwestern Spain, eastern Europe, UK, Belgium and the southwestern Netherlands. These localized industries generate large plumes of high-SO_2 affecting the air quality on a local to regional scale. Background concentrations in eastern countries (8-20 µg m^{-3}) are greater than in West (~2 µg m^{-3}). Various disperse punctual SO_2 emissions in the east contribute to an increase of the regional concentration (30-50 µg m^{-3}). Over sea, the highest concentrations are found along the main shipping route, since fuels used have high-SO_2 content. Comparisons with 31 observed annual means show a high spatial correlation (r = 0.80), resulting from the detailed methodology of spatial (horizontal and vertical) dissagregation of EMEP (50 km x 50 km) data over the high-resolution CALIOPE-EU grid (12 km x 12 km).

In CALIOPE-EU system fine-particle SO_4^{2-} has an anthropogenic origin and is directed emitted, generated by nucleation and/or condensation from the gas phase oxidation of SO_2 and hydroxyl radical (OH) and by heterogeneous oxidation of SO_2 in clouds (aqueous-phase oxidation by H_2O_2, O_3, Fe^{3+} and Mn^{2+}, and peroxyacetic acid) (Binkoswki and Roselle, 2003). With respect to SO_2, SO_4^{2-} presents a pattern more dispersive pattern (lower spatial

variability) since SO_4^{2-} is partly produced during the transport of the SO_2 air masses (Fig. 5b). Regions with high levels of SO_4^{2-} correspond with important SO_2 emission point sources (Fig. 1c and Fig 5a). The highest levels are found in eastern and south-eastern Europe and Po Valley (2 to 5 µg m^{-3}), followed by those obtained over the Benelux region and northeastern Spain (2-3 µg m^{-3}). The highest SO_4^{2-} levels over eastern Europe deplete the available gas-phase NH_3 so that little NH_4NO_3 can form due to the low NH_3 levels as can be seen latter in Fig 5c. These findings are consistent with the results presented in Querol et al. (2009). In remote continental regions SO_4^{2-} mean levels range between 1-2 µg m^{-3}. However, over Scandinavia and elevated terrains (e.g. Alpine and Pyrenean chains) levels remain below 1.0 µg m^{-3}. Over the ocean, fine-particle SO_4^{2-} contributes < 1.5 µg m^{-3} in the Atlantic Ocean and between 1.0 - 2.7 µg m^{-3} over the Mediterranean Sea. The calculated spatial correlation over 53 EMEP stations indicates that there is a high agreement for background annual sulfate levels between CALIOPE-EU and EMEP stations over Europe, indicating that the modeling system is able to reproduce long-range transport, chemical processes and sinks of sulfate.

3.2.2 Nitric acid and nitrate

HNO_3 is produce by heterogeneous hydrolysis of N_2O_5 and by oxidation of NO_2 by hydroxyl radicals (Meng et al. 1997; Nguyen and Dabdub, 2002). According to NO_2 performance, a detail discussion is provided in a separate paper Pay et al. (2010a). However, additional information about NO_2 is provided in the supplementary material. CALIOPE-EU is able to reproduce NO_2 with high good agreement over Europe, with spatial correlation of 0.75 (Fig S1, supplementary material). Nevertheless, NO_2 background levels are significantly underestimated, MB = -3.7 µg m^{-3} (Pay et al., 2010a).

The annual patter of HNO_3 over Europe presents a high spatial variability (Fig. 5c). At continental regions the annual concentrations remain mainly below 1.0 µg m^{-3}, meanwhile over the sea concentrations are larger than those over land. A long the ship routes, where large amount of NO_x are emitted (Fig. 1c), the largest concentrations of HNO_3 are also modeled. Mean values in the Mediterranean Sea are ~ 3 µg m^{-3} reaching maximum levels over the Alboran Sea along the Strait of Gibraltar (~ 5 µg m^{-3}), meanwhile over North Sea and English Channel HNO_3 levels are lower (~ 3 µg m^{-3}). The calculated spatial correlation is 0.63 which is biased by the stations of Illmitz where measurements seem to have more variability during winter than modeled (without Illmitz, the spatial correlation increase to 0.77).

NO_3^- is modeled as NH_4NO_3 in the fine fraction and its formation is bound by NH_4^+ and HNO_3. NO_3^- spatial variability is high over Europe (Fig. 5d) with no clear relationship either anthropogenic activities or gas precursor HNO_3 (Fig. 5c) and NO_2 (Fig S1, supplementary material). Both ammonium nitrate and nitric acid are water soluble and efficiently wet deposited. However, nitric acid is a volatile gas with a rapid dry deposition, meanwhile ammonium nitrate particles dry deposit slowly. NO_3^- levels are significant over land, since NO_3^- concentrations rapidly decrease from the coast to open ocean. NO_3^- presents the highest concentration in the Po valley (between 3 and 4 µg m^{-3}) where both large anthropogenic sources of NO_x and NH_3 from agriculture and industrial-related sources are located. Elevated concentrations are also identified over The Netherland, Belgium, eastern Germany and northern France (~ 2.4 µg m^{-3}) which are affected by high levels of NH_3. Overall, in southern Europe (latitude less than 44°N) NO_3^- concentrations are lower, not exceeding 1.5 µg m^{-3} and remaining below 0.6 µg m^{-3} over the sea. Despite the high HNO_3 levels due to ship tracks over the Mediterranean Sea, NO_3^- concentrations remain low because NH_3 availability is limiting. The annual spatial correlation shows a high agreement between CALIOPE-EU and EMEP observations (r=0.80). Despite such good spatial correlation, modeled background mean NO_3^- levels are somehow underestimated ~ 1 µg m^{-3} over most of the stations as shown in the evaluation section.

Modeled TNO_3 annual distribution (Fig. 5h) shows the sum of contribution of NO_3^- and HNO_3. In continental region, as for NO_3^-, the highest levels are found over the Po valley (~5 µg m^{-3}). Over the sea, the highest values are found along the maritime traffic routes and the Strait of Gibraltar (~4 µg m^{-3}). The spatial correlation for TNO_3 is relatively high (r=0.76), indicating a good agreement between formation of secondary gas and aerosol.

3.2.3 Ammonia and ammonium

Fig. 5e shows annual European pattern of gas-phase NH_3 in 2004. Agriculture and livestock are estimated to produce around 94% of NH_3 emission in Europe (Table 1). Due to the short atmospheric lifetime of ammonia, its concentration field strongly resembles its emission distribution, as shown in Fig. 1a, and maximum concentrations occur in the areas with the highest emissions. Outside the source areas the ammonia concentration declines rapidly (< 1 µg m^{-3}). Maximum concentrations are located in The Netherlands and Po valley (~ 8 µg m^{-3}), followed by southern Germany and western France (~ 5 µg m^{-3}). Significant high levels (2-4 µg m^{-3}) are also found over southwestern France, northeastern Spain, central Poland and

462 southeastern Europe. Comparisons with annual mean observations show high spatial
463 correlation (r=0.93). Nevertheless this correlation is not representative since only seven
464 stations are taking into account.

465 In air masses with a continental signature aerosol NO_3^- and SO_4^{-2} are associated with NH_4^+.
466 Atmospheric NH_3 is first neutralized by H_2SO_4 to form $(NH_4)_2SO_4$. Remaining NH_3 may then
467 combine with HNO_3 to form NH_4NO_3. In this sense, NH_4^+ presents a gradient distribution
468 pattern more similar to SO_4^{2-} and NO_3^- than to NH_3 since NH_4^+ neutralizes those anions (Fig.
469 5f). NH_4^+ concentrations are around 1 µg m^{-3} over most of Europe and decrease near the
470 coast. Like for NO_3^-, the highest NH_4^+ concentrations are detected over the Po Valley (2-3 µg
471 m^{-3}). High NH_4^+ concentrations are also found over the Benelux region and southwestern
472 Europe with values ranging from 1 and 2 µg m^{-3}. Low concentrations are found in southern
473 Europe (<1.2 µg m^{-3}). The low NH_4^+ availability in the southern part of Europe (< 40º N) is
474 mainly used in the neutralization of SO_4^{2-}, meanwhile HNO_3 remains in the gas phase. The
475 lowest concentrations are found in Nordic counties and high mountains ranges (< 0.6 µg m^{-3}).
476 Annual mean spatial correlation shows a high agreement between model and observations
477 (r=0.80).

478 TNO_3 annual distribution is also shown in Fig. 5g; the pattern is obviously dominated by gas-
479 phase NH_3. Spatial correlation for total ammonia is 0.68, lower than for NH_3 and NH_4^+. More
480 stations are used to compute the correlation coefficient for TNH_3, and this result is deviated
481 by the stations of Payerne and Els Torms. Without these two stations spatial correlation
482 increase to 0.71.

483 ## 3.3 Aerosol formation indicators

484 ### 3.3.1 S-ratio

485 The ability of the model to form fine-particle SO_4^{2-} is investigated by the use of the S-ratio
486 indicator (Hass et al., 2003). Fig. 6a presets the annual S-ratio distribution over Europe in
487 2004 modeled with CALIOPE-EU and measured at EMEP stations. Fig. 7c shows the
488 observed and calculated annual S-ratios at each EMEP station lumping by regions (described
489 previously in Table 2 and Fig. 2) and compared with the model performance for SO_2 (Fig. 7a)
490 and SO_4^{2-} (Fig. 7b).

The observed S-ratios range from 0.24 (Tange-DK03) to 0.63 (Sniezka-PL03), meanwhile the modeled S-ratios tend to basically overestimate the observed range due to different regimens dominated in diverse regions. The highest S-ratio (observed and modeled S-ratio > 0.5) are found in eastern Europe and western Iberian Peninsula which indicates that fresh sulfur dominates these regions (oxidation processes are limiting). In this case, CALIOPE-EU overestimates these ratios, which is consistent with the model overestimation of the highest SO_2 levels, especially in eastern Europe (Fig. 7a and Section 3.1.1). S-ratios between 0.4 and 0.5 (modeled and observed) are found over the Mediterranean Basin (C.Med and E.IP-W.Med), central, northwestern, and north Europe (C.Eu, NW.E. and Nor.) where sulfur is dominated by SO_4^{2-} generated during the long-range transport. In this regime, CALIOPE-EU tends to overestimate S-ratio, mainly dominated by the SO_4^{2-} underestimations, which depict deficiencies of the SO_4^{2-} parameterizations (e.g. limitation to the availability of aqueous phase oxidants such as H_2O_2 and ozone as shown in other European studies (Stern et al., 2008; Schaap et al., 2004a; Kim et al., 2011).

The lowest observed and modeled S-ratios (S-ratios < 0.35) are found in northern Europe, at the stations of DK03, DK08 and SE11. Thus, this region is affected by SO_4^{2-} from transport, since no large isolated point sources are located there (Fig. 1a) and is only affected by ship emissions. Under this regime, CALIOPE-EU overestimates these ratios at these three stations, since modeled SO_2 levels are largely overestimated (Fig. 7a). This could indicate that ship emission estimates in the EMEP inventory are too high over these areas as pointed out by Tarrasón et al. (2007).

The spatial correlation is relatively high (r=0.52) since it is biased by the under- and overestimation of sulfur compounds in different regions. Nevertheless, the modeled S-ratio over Europe is consistent with the patterns discussed before for SO_2 and SO_4^{2-}. On one hand, the major shipping routes (from the North Sea, passing by the English Channel, through Portugal, Spain and northern Africa towards the Suez Canal) and power plants in eastern Europe (Poland, Serbia, Rumania, Bulgaria and Greece), northwestern Spain and northwestern Europe (UK, Belgium, The Netherlands) are responsible for fresh sulfur. On the other hand, central Europe and over the Mediterranean Basin are regions affected by the secondary SO_4^{2-} transported form the aforementioned emitted areas which is secondary formed favored by the meteorological pattern (Querol et al. 2009).

3.3.2 Free ammonia

The F-NH_x indicator is a useful tool to identify potential regions with high potential to generate NH_3NO_3, based on the fact that it will be formed if there is enough NH_3 available after the neutralization of the SO_4^{2}. Fig. 6b presets the modeled annual F-NH_x distribution over Europe in 2004. Fig. 8a shows the observed and calculated annual F-NH_x at each EMEP stations lumped by regions.

Observed F-NH_x is in a range of -0.05 to 0.13 µmol m^{-3} (Fig 6c and d). Calculated spatial correlation is relatively high (r=0.65). However, CALIOPE-EU system presents a tendency to overestimate F-NH_x. Under this condition, NH_4NO_3 could be enhanced in the model. Nevertheless, the dominant regimens depend on the region.

Modeled F-NH_x decreases from the coastal areas to the ocean. The lowest (modeled and observed) free ammonia (F-NH_x < 0 µmol m^{-3}) is mainly confined to coastal stations where acid displacements with sea-salt aerosol take place (Athanasopoulou et al., 2009).

Regions with low potentiality to form NH_4NO_3 (0 µmol m^{-3} < F-NH_x < 0.02 µmol m^{-3}) are found in northern Europe and western Iberian Peninsula. In the first case, it is due to the low emissions and gas-phase NH_3 (Fig. 1a and Fig. 6e, respectively). In the second case, despite there is enough NH_3 emission, the elevated S-ratio regime indicates that available NH_3 is partitioned to aerosol phase to neutralized SO_4^{2-}.

Regions with relatively high potentiality to form NH_4NO_3 (0.02 µmol m^{-3} < F-NH_x < 0.04 µmol m^{-3}) are eastern Iberian Peninsula and eastern Europe. In both cases, NH_3 emissions are high (100-250 Mg/yr and small areas 250-450 Mg/yr). CALIOPE-EU tends to underestimate F-NH_x over Iberian Peninsula since TNH_3 are underestimated.

The highest measured and observed F-NH_x (F-NH_x > 0.04 µmol m^{-3}) are found in central (south Germany and Po valley) and northwestern Europe (Benelux and eastern France) where the highest and extended NH_3 emissions (>1,400 Mg/yr) together with meteorological conditions (low temperature and high relatively humidity) favored the partition of NO_3^- to aerosol phase. In this case, CALIOPE-EU tends to overestimate the highest F-NH_x since TNH_3 are overestimated in those areas.

3.3.3 G-ratio

Fig. 6c shows the annual distribution pattern of observed and calculated G-ratios over 2004. G-ratio is useful to analyze which reactant, NH_3 or HNO_3, limits the formation of NH_4NO_3 (Ansari and Pandis, 1998). Fig. 8c shows the observed and calculated annual G-ratio at each EMEP stations compared with the performance of F-NH_x (Fig. 8a) and TNO_3 (Fig. 8b).

The modeled and observed spatial distribution of G-ratio indicates that, based on annual average concentration, over continental Europe the NH_4NO_3 formation is limited by the formation of HNO_3 (G-ratio > 1). Adams et al. (1999) showed the same tendency over the European continent using the global model GISS GCM II. Also Sartelet et al. (2007) and Kim et al. (2011) estimated the same pattern over continental areas with the POLYPHEMUS system using different chemical mechanisms (CB05 and RACM). Such findings indicate that NH_4NO_3 concentration in these areas could increase dramatically given an increase in HNO_3 concentration, or indirectly given an increase of NO_x emissions. It is also consistent with results obtained by Renner and Wolke (2010) over northwestern Europe, who demonstrate that ammonium nitrate, but above all ammonium sulfate, is not sensitive to NH_3 emission changes when SO_2 and NO_x are limiting.

Over ocean, NO_3^- is produced over the English Channel, Atlantic coast of France, and the North Sea, although NH_3 limits its formation (0 < G-ratio < 1). An acidic sulfate aerosol dominates the Mediterranean Sea (G-ratio < 0) severely limited by NH_3, where intense maritime traffic generate high NO_x (indirectly HNO_3) and SO_2 emissions.

The low spatial correlation (r = 0.27) are related with the fact that this equation may be too simplistic for location where NO_3^- is often neutralized by sodium or calcium, such as coastal areas or western Mediterranean Basin (Querol et al., 2009). Even though, CALIOPE-EU system estimates sea-salt emissions; however, replacement of chloride by nitrate in mixed marine/urban air masses is not implemented in AERO4 (Kelly et al., 2010).

4 Comparison with other AQM evaluation studies

Recent AQM studies have provided more insight in the SIA formation in Europe. This section discusses a comparative analysis between various European model evaluations and the results obtained here form the CALIOPE-EU system. Note that this is not an exhaustive inter-comparison study because of the different configuration of the diverse works. Nevertheless, it

580 provides a good basis for assessing the reliability of the results obtained in the context of the
581 European model evaluation which also complement that presented in Pay et al. (2010a). Table
582 4 shows a chronological list of published AQM evaluation studies on SIA and precursors
583 gases, which are presented along with CALIOPE-EU evaluation results. Following the criteria
584 in Pay et al. (2010a) those evaluation studies have several characteristics in common: (1)
585 European domain; (2) the regional scale (horizontal resolutions are between 12 km to 55 km);
586 (3) the simulation period, mainly annual, except in the case of Kim et al. (2011) and Stern et
587 al. (2008); and (4) the used of the EMEP monitoring network to evaluate the models. Table 5
588 presents the common statistics for the fine inorganic aerosols (SO_4^{2-}, NO_3^- and NH_4^+). Gas-
589 phase aerosol precursors (nitric acid and ammonia) and total nitrate and ammonia are
590 presented in Table 6. Results for sulfur dioxide are presented at Table 5 in Pay et al. (2010a).
591 Three common statistics parameters are considered: the ratio between modeled mean and
592 observed mean (Ratio), correlation coefficient (r), and RMSE.

593 For SO_4^{2-} concentration CALIOPE-EU presents satisfactory annual correlations in
594 comparison to the other studies (0.49 versus 0.37-0.65 in annual basis). However, the RMSE
595 obtained with CALIOPE-EU is the lowest form all the models (1.3 µg m^{-3} for CALIOPE-EU
596 versus 1.7-5.89 µg m^{-3}). As other European modeling system, CALIOPE-EU tends to
597 underestimate SO_4^{2-} annual concentrations.

598 Considering NO_3^-, the annual correlation obtained for CALIOPE-EU (r = 0.58) is, with
599 LOTOS8, the third highest value after EURAD9 (r=0.61) and the EMEP6 (r = 0.80). Note
600 that EMEP6 presented also the highest correlation for NO_2 (Pay et al., 2010a). The other
601 studies calculated lower correlations for nitrate ranging from 0.17 to 0.50. The RMSE for
602 CALIOPE-EU are in the low range from the other studies (2.30 µg m^{-3} against 1.59-6.39 µg
603 m^{-3}). Differently from the other European modeling system, CALIOPE-EU tends to simulates
604 slightly lower aerosol nitrate concentrations than those measured presenting the lowest Ratio
605 (Ratio = 0.50), closely followed by CMAQ3 (Ratio = 0.63).

606 As for NO_3^-, the annual correlation for NH_4^+ obtained within CALIOPE-EU (r = 0.62) is the
607 same as for LOTOS8, and the second highest value after EMEP6 (r = 0.82). The other studies
608 present lower correlations but always higher than those obtained for NO_3^- (0.39-0.61). RMSE
609 for CALIOPE-EU is in the same range as the other studies (1.20 µg m^{-3} against 0.83-2.90 µg
610 m^{-3}). Again, conversely from the other studies, CALIOPE-EU tends to underestimate NH_4^+,

presenting the second lowest Ratio (Ratio = 0.67), after MATCH9 (Ratio = 0.55) and relatively closer to CMAQ3 (Ratio = 0.75).

As discussed in Pay et al. (2010a), the CALIOPE-EU evaluation results for SO_2 show very satisfactory performances in comparison with other studies, mainly attributed to the high resolution of the CALIOPE-EU system which enables a well-defined spatial and temporal description of SO_2 sources over Europe. As CALIOPE-EU most of the European models present the a tendency to overestimate SO_2, e.g. bias of 1.3 $\mu g\ m^{-3}$ for CALIOPE-EU versus biases between 1.0 and 2.3 $\mu g\ m^{-3}$ for EUROTRAC models (Hass et al., 2003). For HNO_3, not too much comparison can be done since there are only few stations that measured this compound. Annual correlation coefficient is higher than that presented in other studies (0.41 for CALIOPE-EU versus 0.26 (POLYPHEMUS5) - 0.38 (EMEP6)). RMSE is in the same range than that obtained POLYPHEMUS5.

Overall, CALIOPE-EU performances for NH_3 are superior to other European studies. The correlation obtained is this study is the highest from all considered models (0.56 against 0.05-0.33). The RMSE is in the lowest range from other European studies (1.1 $\mu g\ m^{-3}$ for CALIOPE-EU versus 5.40 -7.50 $\mu g\ m^{-3}$). As other European studies, the CALIOPE-EU system tends to underestimate NH_3 in the gas phase (0.77 against 0.18-0.85). Given the strong gradients in NH_3 levels, the high resolution of CALIOPE-EU, both vertical and horizontal, could justify its better skills to reproduce the large NH_3 gradients compared to other European models (Asman, 2001).

For TNO_3, correlations are in the same range of the other European studies (0.50 for CALIOPE-EU against 0.37-0.56). Only EMEP6 is out the mean (r = 0.87) consistently with its highest correlation for NO_3^-. RMSE for all the models is in the same range (2.1 for CALIOPE-EU versus 1.80 $\mu g\ m^{-3}$ - 3.70 $\mu g\ m^{-3}$). Similar results for TNO_3 are found in LOTOS8 for correlation (0.50 against 0.52), RMSE (2.1 $\mu g\ m^{-3}$ against 2.3 $\mu g\ m^{-3}$), and a similar tendency to underestimate TNO_3 (Ratio = 0.77 vs. Ratio = 0.81). As for TNO_3, statistics for TNH_3 modeled by CALIOPE-EU system is in the range of other studies.

The different performance of SIA and precursor gases seems to be related with the chemical mechanism and thermodynamic equilibrium. Most of European models in this comparison used the Carbon Bond IV chemical mechanism. The CB-IV has recently been updated, namely CB05 (Yarwood et al., 2005). Yu et al. (2010) found that CB05 has the relatively

642 better performance for HNO_3 and SO_2 than for CB-IV. This update is interesting since, as
643 showed before, nitrate formation tends to be HNO_3-limited over continental areas. Recently,
644 Kim et al. (2011) tested the impact of RACM2 (updated version of RACM, Goliff and
645 Stocwell, 2010) and CB05 on the formation of SIA over Europe and showed that differences
646 in SIA result from differences in oxidant concentration (OH, O_3 and NO_3).

647 According to the thermodynamic equilibrium, EQSAM module (Metzger et al., 2002) is
648 widely used in EMEP model and global models (MATCH and DEHM). This module is very
649 simplified and tends to partition too much NO_3^- and NH_4^+ to aerosol phase under lower
650 temperatures (Tarrasón et al., 2006) causing the aforementioned overestimation of these
651 species. ISORROPIA has proved to be the model of choice for many three-dimensional air
652 quality models in Europe due to its computationally efficient and rigor. An important
653 limitation of ISORROPIA is the lack of treatment of crustal species (Ca, K, Mg), important in
654 simulating the partitioning of NO_3^- and NH_4^+, especially in areas like the southern Europe
655 where dust (from deserts or resuspended form arid areas) comprise a significant portion of
656 PM10 and PM2.5 (Querol et al., 2009). Recently, an update version of ISORROPIA that
657 includes crustal species has been published, namely ISORROPIA II (Fountoukis and Nenes,
658 2007).

659 # 5 Summary and Conclusion

660 This paper present an evaluation of the results of the CALIOPE-EU high-resolution modeling
661 system (12 km x 12 km, 1hr) in terms of secondary inorganic aerosol (SIA) (SO_4^{2-}, NO_3^- and
662 NH_4^+) and its gas precursors (SO_2, HNO_3 and NH_3) using a full- year simulation for 2004
663 over Europe. Modeling results have been compared to long-term surface concentration from
664 the EMEP monitoring network and to other European evaluation studies. The evaluation is
665 focused on the capability of the model to reproduce (1) the temporal and spatial distribution
666 of SIA and its precursors, in terms of statistics; and (2) the inorganic aerosol formation
667 regimens, in terms of so-called indicators, over Europe.

668 CALIOPE-EU presents a high accuracy for reproducing SIA levels and (spatial and temporal)
669 variability. Although the total amount of SIA is on average underestimated by 18-50% in
670 most regions of Europe, the temporal variability and hence the transport patterns of these
671 species are captured rather well, as indicated by the correlation coefficients, which range
672 between 0.49 and 0.62. Taking into account that natural sources of SIA precursors are not

673 considered in the emissions this result is satisfying. Performance for N-compounds gas
674 precursor species (nitric acid and ammonia) is not as accurate as for aerosol based on
675 fractional biases and errors.

676 Results indicate that there is no significant relationship between SIA evaluation and
677 performance for gas-phase precursors. SO_2 is systematically over-predicted by CALIOPE-EU
678 system. Since SO_2 emissions are dominated by large electrical power plants and they are
679 traditionally well understood, deposition mechanism and meteorological performances could
680 be responsible from this underestimation. Overall, the positive mean bias for only SO_2
681 suggests that non-marine SO_4^{2-} formation in the modeling system is often limited by oxidant
682 availability and not always by sulfur dioxide availability.

683 Overall NO_3^- concentrations are underestimated in -60% in winter and < -100% in summer.
684 The uncertainty of NO_3^- and HNO_3 measurements hampers to discern if the model
685 overestimation of HNO_3, especially in summer, results from deficiency in model-process
686 description. The summer overestimation of HNO_3 and underestimation of NO_3^- should have
687 minimal impact on regulatory applications since the warm temperatures do not favor the
688 ammonium nitrate formation.

689 Simulated NH_4^+ concentrations were generally underestimated (~ 20%). Two factors that
690 most strongly influence simulated NH_4^+ concentration in Europe are NH_3 emissions and SO_4^{2-}
691 concentration. Modeled NH_3 does not compare as well with observation as NH_4^+ does. The
692 modeled NH_3 concentrations are underestimated by ~100% during summer.

693 SIA and its gas precursors have been also analyzed in terms of goals and criteria following
694 Boylan and Russell (2006). SO_2/SO_4^{2-} and TNH_3/NH_4^+ monthly concentrations accomplish
695 the criteria for bias and errors. TNO_3 falls within the criteria in warm seasons for biases and
696 errors. The larger errors and fraction biases are found for HNO_3 and NO_3^-.

697 Fine-particle SO_4^{2-} shows a lower spatial variation which indicates that it is produced mainly
698 from cloud processing over large scales rather than from direct gas phase oxidation of SO_2.
699 SO_4^{2-} presents a clear west-east gradient over Mediterranean Basin, dominated by the large
700 isolated sources located in eastern Europe. In contrast with SO_4^{2-}, NO_3^- presents a prominent
701 east-west and south-north increasing gradient over Europe. Special features may account for
702 these differences: (1) the high levels of SO_4^{2-} in eastern Europe depletes the available gas-
703 phase NH_3 so that little NH_4NO_3 can form in this region due to the low NH_3 levels, and (2)

704 the higher ambient temperature in the south favors the gas phase prevalence of NO_3^-.
705 Concerning NH_4^+, concentrations patterns shows low variability and it follows NO_3^- and SO_4^{2-}
706 concentrations.

707 HNO_3 levels decrease over land and increase over the oceans. Despite the high HNO_3 levels
708 due to ship tracks over the Mediterranean Sea, NO_3^- concentrations remain low because NH_3
709 availability is limiting. Gas-phase NH_3 concentrations are high in continental areas with high
710 NH_3 emissions, particularly if little SO_4^- is present. NH_3 concentrations are found to be
711 highest regionally in UK, The Netherlands, southwestern France, the Po valley, central
712 Poland, southeastern Europe and southern Sweden.

713 Modeled and observed S-ratios indicates that fresh sulfur dominate eastern Europe, western
714 Iberian Peninsula, and the major shipping routes, where oxidants are limiting the formation of
715 sulfate. On the other hand, central Europe and the Mediterranean Basin are regions affected
716 by the secondary SO_4^{2-} transported form the aforementioned emissions. The free ammonia
717 indicator estimated by CALIOPE-EU system tends to agree with the observed estimations and
718 improves the confidence on the fact that modeled nitrate will respond appropriately to change
719 in precursor emissions.

720 Fine-particle nitrate formation is mostly limited by the availability of HNO_3 over continental
721 region in Europe. Based on the analysis of the three studied indicators (S-ratio, F-NH_x and G-
722 ratio) formation of SIA in Europe tends to be limited by precursors SO_2 and HNO_3 due to the
723 relatively high NH_3 emission, mainly from agriculture, especially in northwestern Europe.
724 Regulatory strategies in this part of Europe should focus on the reduction of NO_x and SO_2
725 rather than in NH_3 to control ammonium nitrate and ammonium sulfate, respectively.

726 The comparison with previous modeling results suggest that CALIOPE-EU performs
727 relatively well for NH_4NO_3 concentrations while high scores were obtained for SO_4^{2-}, and
728 gas-phase aerosol precursors (SO_2, HNO_3 and NH_3). However, substantial efforts should be
729 made in the temporal description of NH_3 emissions, which determinates the formation of
730 ammonium sulfate and gas-aerosol partitions. The correlations of primary gases (SO_2 and
731 HN_3, and also NO_2) are notably higher for CALIOPE-EU than for other European system.
732 Most models are based on EMEP emission inventory, but the disaggregation methodologies
733 are different in each case. The higher horizontal resolution and the detailed disaggregation
734 techniques of CALIOPE-EU system may be responsible for the better scores obtained in SO_2.

The horizontal resolution may impact urban and industrial areas at a higher degree than rural areas. In this sense, the higher horizontal resolution of CALIOPE-EU system may be responsible for the better scores obtained for NO_2 and SO_2. It is reasonable to think that a detailed emission inventory at a finer horizontal resolution could further improve the air quality model performances.

Another relevant issue it that arises from the model comparison is the impact of vertical resolution. Models presented in this evaluation ranges from 3 to 20 vertical layers. It is expected that models with higher vertical levels are able to simulate the vertical mixing better, especially for NH_3 which is shown to have a high vertical gradient (Schaap et al., 2004a).

Overall, the performances on the gas-phase precursor gases (HNO_3 and NH_3) and fine-particle NH_4NO_3 are relatively poor, but the intercomparison detailed in this work shows that the uncertainties and the lack of understanding around nitrate compounds is a general feature affecting most models. On the other hand, the model performance for SO_4^{2-} is better. The emissions of SO_2 are rather well known and the formation of SO_4^{2-} is not as complex as for NH_4NO_3; also a long history of research has been devoted to this component.

Furthermore, modeling evaluation of in terms of indicators suggests that CALIOPE-EU system is appropriate for regulatory modeling applications. Nevertheless, it is important to continue to examine CALIOPE-EU performance for these chemical species and their precursors to continue to improve model estimates of these species. The results of this study suggest several points for future research devoted to this topic, which are presently being implemented:

- A better characterization of NH_3 emission factors according to inter-annual variability.
- An increase of the spatial coverage and reliability of data sets on NO_3^-, HNO_3 , NH_3 and NH_4^+, which allow a full evaluation of photochemical model results.
- Implement ISORROPIA II thermodynamic equilibrium, allowing an accurate representation of nitrate since it includes interaction with crustal material.
- Implement the update version of the chemical mechanism CB05.
- Implement biomass burning and natural NO_x emissions (e.g. lightnings, soils) which could contribute to the underestimation of N-compounds.

Acknowledgements

The authors wish to thank EMEP for the provision of measurements stations. This work is funded by the CALIOPE project of the Spanish Ministry of the Environment (441/2006/3-12.1, A357/2007/2-12.1, 157/PC08/3-12.0) and the project CICYT CGL2006-11879 and CGL2008-02818 of the Spanish Ministry of Education and Science. P. Jiménez-Guerrero acknowledges the Ramón y Cajal Programme of the Spanish Ministry of Science and Technology. The Spanish Ministry of Science and Innovation is also thanked for the Formación de Personal Investigador (FPI) doctoral fellowship held by María Teresa Pay (CGL2006-08903). All simulations were performed on the MareNostrum supercomputer hosted by the Barcelona Supercomputing Center.

References

Adams, P.J., Seinfeld, J.H., Koch, D.M., 1999. Global concentrations of tropospheric sulfate, nitrate, and ammonium aerosol simulated in a general circulation model. J. Geophys. Res., 104, 13791-13823.

Altshüller, A.P., 1984. Atmospheric particle sulfur and sulfur dioxide relationships at urban and nonurban locations. Atmos. Enrivon., 18, 1421-1431.

Ansari, A.S., Pandis, S., 1998. Response of inorganic PM to precursor concentrations. Environ. Sci. Technol., 32, 2706-2714.

Appel, K.W., Bhave, P.V., Gilliland, A.B., Sarwar, G., Roselle, S.J., 2008. Evaluation of the community multiscale air quality (CMAQ) model version 4.5: Sensitivities impacting model performance; Part II-particulate matter. Atmos. Environ., 42, 6057-6066.

Asman, W.A.H., 2001. Modelling the atmospheric transport and deposition of ammonia and ammonium: an overview with special reference to Denmark. Atmos. Envrion., 35, 1969-1983.

Athanasopoulou, E., Tombrou, M., Pandis, S.N., Russell, A.G., 2008. The role of sea-salt emissions and heterogeneous chemistry in the air quality of polluted coastal areas. Atmos. Chem. Phys., 8, 5755-5769.

Baldasano, J.M., Jiménez-Guerrero, P., Jorba, O., Pérez, C., López, E., Güereca, P., Martín, F., Vivanco, M.G., Palomino, I., Querol., X., Pandolfi, M.J., Sanz, M., Diéguez, J.J., 2008a. Caliope: an operational air quality forecasting system for the Iberian Peninsula, Balearic islands and Canary islands –first annual evaluation and ongoing developments. Adv. Sci. Res., 2, 89-98.

Baldasano J.M., L. P. Güereca, E. López, S. Gassó, P. Jimenez-Guerrero, 2008b. Development of a high-resolution (1 km x 1 km, 1 h) emission model for Spain: the High-Elective Resolution Modeling Emission System (HERMES). Atmos. Environ., 42 (31), 7215-7233.

Baldasano, J.M., Pay, M.T., Jorba, O., Gassó, S., Jiménez-Guerrero, P., 2011. An annual assessment of air quality with the CALIOPE modeling system over Spain. Sci. Total Environ., 409, 2163-2178.

803 Baker, K., Scheff, P., 2007. Photochemical model performance for PM2.5 sulfate, nitrate,
804 ammonium, and precursor species SO_2, HNO_3, and NH_3 at background monitor locations in
805 the central and eastern United States. Atmos. Environ., 41, 6185-6195.

806 Bessagenet, B., Hodzic, A., Vautard, R., Beekmann, M., Cheinet, S., Honoré, C., Liousse, C.,
807 Rouïl, L., 2004. Aerosol modeling with CHIMERE-preliminary evaluation at the continental
808 scale. Atmos. Environ., 38, 2803-2817.

809 Binkowski, F., Shankar, U., 1995. The regional particulate matter model 1. Model description
810 and preliminary results. Journal of Geophysical Research 100 (D12), 26191-26209.

811 Binkowski, F. S., Roselle, S. J., 2003. Models-3 Community Multiscale Air Quality (CMAQ)
812 model aerosol component: 1. Model description. J. Geophys. Res., 108(D16), 4183.

813 Boylan, J. W., Russell, A. G., 2006. PM and light extinction model performance metrics,
814 goals, and criteria for three-dimensional air quality models. Atmos. Environ., 40(26), 4946-
815 4959.

816 Bytnerowicz, A., Omasa, K., Paoletti, E., 2007. Integrated effects of air pollution and climate
817 change on forests: A northern hemisphere perspective. Envion. Poll., 147, 438-445.

818 Byun, D., Schere, K.L., 2006. Review of the foverning equations, computational algorithms,
819 and other components of the models-3 community multiscales air quality (CMAQ) modeling
820 system. Appl. Mech. Rev., 59 (2), 51-77.

821 Dennis, R., Fox, T., Fuentes, M., Gilliland, A., Hanna, S., Hogrefe, C., Irwin, J., Rao, S.T.,
822 Scheffe, R., Schere, K., Steyn, D., Venkatram, A., 2010. A framework for evaluating
823 regional-scale numerical photochemical modeling systems. Environ. Fluid Mech. doi:
824 10.1007/s10652-009-9163-2.

825 EEA, 2000. CORINE Land Cover, 2000. Technical Report. European Environmental Agency.
826 Available at: http://dataservice.eea.eu.int/dataservice.

827 EMEP, 2004. EMEP Assessment Part I. In: Lövblad, G., Tarrasón, L., Torseth, K., Dutchak,
828 S. (Eds.), European Perspective. Available at: www.emep.int.

829 EMEP, 2007. National Emissions Reported to the Convention on Long-range Transboundary
830 Air Pollution (LRTAP Convention). Air Emission Annual Data Reporting (EMEP/MSC-W).

831 Technical Report. European Environmental Agency, The Norwegian Meteorological Institute,
832 Oslo, Norway.

833 European Commission, 2008. Directive 2008/50/EC of the European Parliament and of the
834 Council of 21 May 2008 on Ambient Air Quality and Cleaner Air for Europe. Technical
835 Report 2008/50/EC, L152. Off. J. Eur. Comm.

836 Fagerli, H., Aas, W., 2008. Trends of nitrogen in air and precipitation: Model results and
837 observations at EMEP sites in Europe, 1980-2003. Environ. Pol., 154, 448-461.

838 Fountoukis, C., Nenes, A., 2007. ISORROPIA II: a computationally efficient thermodynamic
839 equilibrium model for K^+-Ca_2^+-Mg_2^+-NH_4^+-Na^+-SO_4^{2-}-NO_3^--Cl^--H_2O aerosols. Atmos. Chem.
840 Phys., 7, 4639-4659.

841 Gery, M.W., Whitten, G.Z., Killus, J.P., Dodge, M.C., 1989. A photochemical kinetics
842 mechanism for urban and regional scale computer modeling. J. Geophys. Res., 94(D10),
843 12925-12956.

844 Gilliland, A.B., Dennis, R.L., Roselle, S.J., Pierce, T.E., 2003. Seasonal NH_3 emission
845 estimates for the eastern United States based on ammonium wet concentrations and an inverse
846 modeling method. J. Geophys. Res., 108(D15), 4477. doi:10.1029/2002JD003063.

847 Gilliland, A. B., Gilliland, Appel, W.K., Pinder, R.W., Dennis, R.L., 2006. Seasonal NH_3
848 emissions for the continental united states: Inverse model estimation and evaluation. Atmos.
849 Environ., 40, 4986-4998.

850 Gonçalves, M., Jiménez-Guerrero, P., López, E., Baldasano, J.M., 2008. Air quality models
851 sensitivity to on-road traffic speed representations: Effects on air quality of 80 km h^{-1} speed
852 limit in the Barcelona Metropolitan area. Atmos. Environ., 42, 8389-8402.

853 Gonçalves, M., Jiménez-Guerrero, P., Baldasano, J.M., 2009a. Contribution of atmospheric
854 processes affecting the dynamics of air pollutions in South-Western Europe during a typical
855 summertime photochemical episode. Atmos. Chem. Phys., 9, 849-864.

856 Gonçalves, M., Jiménez-Guerrero, P., Baldasano, J.M., 2009b. High-resolution modeling of
857 the effects of alternative fuels use on urban air quality: Introduction of natural gas vehicles in
858 Barcelona and Madrid Greater Areas (Spain). Sci. Total Environ., 407, 776-790.

Goliff, W.S., and Stocwell, W.R., 2010. The Regional Atmospheric Chemistry Mechanism, version 2.1. Description and Evaluation. J. Geophys. Res. Submitted 2010.

Hamed, A., Birmili, W., Joutsensaari, J., Mikkonen, S., Asmi, A., Wehner, B., Spindler, G., Jaatinen, A., Wiedensohler, A., Korhonen, H., Lehtinen, K.E., Laaksonen, A., 2010. Changes in the production rate of secondary aerosol particles in Central Europe in view of decreasing SO_2 emissions between 1996 and 2006. Atmos. Chem. Phys., 10, 1071-1091.

Hass, H., van Loon, M., Kessler, C., Stern, R., Matthijsen, J., Sauter, f., Zlatev, Z., Langner, J., Foltescu, V., Schaap, M., 2003. Aerosol Modeling: Results and Intercomparison from European Regional Scale Modeling System. Technical Report. EUROTRAC 2 Report, EUREKA Environmental Project, GLOREAM.

Hinneburg, D., Renner, E., Wolke, R., 2007. Formation of secondary inorganic aerosols by power plant emissions exhausted through cooling towers in Saxony. Environ. Science Poll. Res., 16, 25-35.

IPCC, 2007. Climate Change 2007: The Physical Science Basis. Contribution of Working Group I to the Fourth Assessment Report of the IPCC (ISBN 978 0521 88009-1 Hardback; 978 0521 70596-7 Paperback).

Jiménez, P., Baldasano, J.M., Dabdub, D., 2003. Comparison of photochemical mechanisms for air quality modeling. Atmos. Environ., 37 (30), 4179-4194. doi:10.1016/S1352-2310(03)00567-3.

Jiménez, P., Parra, R., Gassó, S., Baldasano, J.M., 2005a. Modeling the ozone weekend effect in very complex terrains: a case study in the northeastern Iberian Peninsula. Atmos. Environ., 39, 429-444.

Jiménez, P., Jorba, O., Parra, R., Baldasano, J.M., 2005b. Influence of high-model grid resolution on photochemical modeling in very complex terrains. Int. J. Environ. Pollut., 24, 180-200.

Jiménez, P., Jorba, O., Parra, R., Baldasano, J.M., 2006a. Evaluation of MM5-EMICAT2000-CMAQ performance and sensitivity in complex terrain: High-resolution application to the northeastern Iberian Peninsula. Atmos. Environ., 40, 5056-5072.

887 Jiménez, P., Lelieved, J., Baldasano, J.M., 2006b. Multi-scale modeling of air pollutants
888 dynamics in the northwestern Mediterranean basin during a typical summertime episode. J.
889 Geophys. Res. 111(D18306), 1-21. doi:10.1029/2005JD006516.

890 Jiménez, P., Parra, R., Baldasano, J.M., 2007. Influence of initial and boundary conditions for
891 ozone modeling in very complex terrains: A case study in the northeastern Iberian Peninsula.
892 Environ. Modell. Softw., 22, 1294-1306.

893 Jiménez-Guerrero, P., Pérez, C., Jorba, O., Baldasano, J.M., 2008a. Contribution of Saharan
894 dust in an integrated air quality system and its on-line assessment. Geophys. Res. Lett.,
895 35(L03814). doi:10.1029/2007GL031580.

896 Jiménez-Guerrero, P., Jorba, O., Baldasano, J.M., Gassó, S., 2008b. The use of a modelling
897 system as a tool for air quality management: annual high resolution simulation and evaluation.
898 Sci. Total Environ., 390, 323-340.

899 Kasibhatla, P., Chameides, W. L., Jonn, J.S., 1997. A three dimensional global model
900 investigation of seasonal variations in the atmospheric burden of anthropogenic sulphate
901 aerosols. J. Geophys. Res., 102, 3737-3759.

902 Kelly, J.T., Bhave, P.V., Nolte, C.G., Shankar, U., and Foley, K.M., 2010. Simulating
903 emission and chemical evolution of coarse sea-salt particles in the Community Multiscale Air
904 Quality (CMAQ) model. Geosci. Model Dev., 3, 257-273, doi:10.5194/gmd-3-257-2010.

905 Kim, Y., Sartelet, K., Seigneur, C., 2011. Formation of secondary aerosols over Europe:
906 comparison of two gas-phase chemical mechanisms. Atmos. Chem. Phys., 11, 538-598.

907 Matthias, V., 2008. The aerosol distribution in Europe derived with the Community
908 Multiscale Air Quality (CMAQ) model: comparison to near surface in situ and sunphotometer
909 measurements. Atmos. Chem. Phys., 8, 5077-5097.

910 Meng, Z., Dabdub, D., Seinfeld, J.H., 1997. Chemical coupling between atmospheric ozone
911 and particulate matter. Science, 277, 116-199.

912 Metzger, S.M., Dentener, F.J., Lelieveld, J., Pandis, S.N., 2002. Gas/aerosol partitioning I: a
913 computationally efficient model. J. Geophys. Res., 107, 109-132.

914 Michalakes, J., Dudhia, J., Gill, D., Henderson, T., Klemp, J., Skamarock, W., Wang, W.,
915 2004. The weather research and forecast model: software architecture and performance. In:
916 Mozdzynski, E.G. (Ed.), To Appear in Proceeding of the Eleventh ECMWF Workshop on the
917 Use of High Performance Computing in Meteorology, 25-29 October 2004, Reading, U.K. pp.
918 117-124.

919 Nenes, A., Pilinis, C., Pandis, S.N., 1998. ISORROPIA: a new thermodynamic equilibrium
920 model for multiphase multicomponent inorganic aerosols. Aquat. Geochem. 4 (1), 123-152.
921 doi:10.1023/A:1009604003981.

922 Nguyen, K., and Dabdub, D., 2002. NO_x and VOC control and its effects on the formation of
923 aerosols. Aerosol Science and Tech., 36, 560-572.

924 Niyogi, D., Chang, H.I., Saxena, V.K., Holt, T., Alapaty, K., Booker, F., Chen, F., Davis,
925 K.F., Holben, B., Matsui, T., Meyers, T., Oechel, W.C., Pielke, R.A., Wells, R., Wilson, K.,
926 Xue, Y., 2004. Directs obervations of the effects of aerosol loading on net ecosystem CO_2
927 exhanges over different landscapes. Geo. Res. Lett., 31. doi: 10.1029/2004GL020915.

928 Pay, M.T., Piot, M., Jorba, O., Gassó, S., Gonçalves, M., Basart, S., Dabdub, D., Jiménez-
929 Guerrero, P., Baldasano, J.M., 2010a. A full year evaluation of the CALIOPE-EU air quality
930 modeling system over Europe for 2004. Atmos. Environ., 44, 3322-3342.

931 Pay, M.T., Jiménez-Guerrero, P., Baldasano, J.M., 2010b. Implementation of resuspension
932 from paved roads for the improvement of CALIOPE air quality system in Spain. Atmos.
933 Environ., 45, 802-807. doi: 10.1016/j.atmosenv.2010.10.032.

934 Pinder, R.W., Dennis, R.L., Bhave, P.V., 2008. Observable indicators of the sensitivity of
935 PM2.5 nitrate to emission reductions-Part I: Derivation of the adjusted gas ratio and
936 applicability at regulatory-relevant time scales. Atmos. Environ., 42, 1275-1286.

937 Piot, M., Jorba, O., Jiménez, P., Baldasano, J.M., 2008. The role of lateral boundary
938 conditions and boundary layer in air quality modeling system. Eos Trans. AGU 8, H212+,
939 Abstract A41H-0212.

940 Pope, C.A.I., Ezzati, M., Dockery, D.W., 2009. Fine-particulate air pollution and life
941 expectancy in the United States. N. Engl. J. Med. 360, 376-386.

Putaud, J.-P., Raes, F., van Dingenen, R., Brüggemann, E., Facchini, M.-C., Decesari, S., Fuzzi, S., Gehrig, R., Hüglin, C., Laj, P., Lorbeer, G., Maenhaut, W., Mihalopoulos, N., Müller, K., Querol, X., Rodriguez, S., Schneider, J., Spindler, G., ten Brink, H., Torsenth, K., Wiedensohler, A., 2004. A European aerosol phenomenology-2: chemical characteristics of particulate matter at kerbside, urban, rural and background sites in Europe. Atmos. Environ., 38, 2579-2595.

Putaud, J.-P., van Dingenen, R., Alastuey, A., Bauer, H., Birmili, W., Cyrys, J., Flentje, H., Fuzzi, S., Gehrig, R., Hansson, H., Harrison, R., Herrmann, H., Hitzenberger, R., H¨uglin, C., Jones, A., Kasper-Giebl, A., Kiss, G., Kousa, A., Kuhlbusch, T., Löschau, G., Maenhaut, W., Molnar, A., Moreno, T., Pekkanen, J., Perrino, C., Pitz, M., Puxbaum, H., Querol, X., Rodriguez, S., Salma, I., Schwarz, J., Smolik, J., Schneider, J., Spindler, G., ten Brink, H., Tursic, J., Viana, M., Wiedensohler, A., and Raes, F., 2010. A European aerosol phenomenology - 3: Physical and chemical characteristics of particulate matter from 60 rural, urban, and kerbside sites across Europe, Atmos. Environ., 44, 1308–1320, doi:10.1016/j.atmosenv.2009.12.011.

Querol, X., Alastuey, A., Ruiz, C.R., Artiñano, B., Hansson, H.C., Harrison, R.M., Buringh, E., ten Brink, H.M., Lutz, M., Bruckmann, P., Straehl, P., Schneider, J., 2004. Speciation and origin of PM10 and PM2.5 in selected European cities. Atmos. Environ., 38, 6547-6555.

Querol, X., Pey, J., Pandolfi, M., Alastuey, A., Cusack, M., Pérez, N., Moreno, T., Viana, M., Mihalopoulos, N., Kallos, G., Kleanthous, S., 2009. African dust contributions to mean ambient PM10 mass-levels across the Mediterranean Basin. Atmos. Environ., 43, 4266-4277.

Renner, E., Wolke, R., 2010. Modelling the formation and atmospheric transport of secondary inorganic aerosols with special attention to regions with high ammonia emissions. Atmos. Environ., 44, 1904-1912.

Roy, B., Mathur, R., Gilliland, A.B., Howard, S.C., 2007. A comparision of CMAQ-based aerosol properties with IMPROVE, MODIS, and AERONET data. J. Geophys. Res., 112 (D14301). doi: 10.1029/2006JD008085.

Sartelet, K.N., Debry, E., Fahey, K., Roustan, Y., Tombette, M., Sportisse, B., 2007. Simulation of aerosols and gas-phase species over Europe with the POLYPHEMUS system: Part I-Model-to-data comparison for 2001. Atmos. Environ., 41, 6116-6131.

Schaap, M., van Loon, M., ten Brink, H.M., Dentener, F.J., Builtjes, P.J.H, 2004a. Secondary inorganic aerosol simulations for Europe with special attention to nitrate. Atmos. Chem, Phys., 4, 857-874.

Schaap, M., Spindler, G., Schulz, M., Acker, K., Maenhaut, W., Berner, A., Wieprecht, W., Streit, N., Müller, K., Brüggemann, E., Putaud, J.-P., Puxbaum, H., Baltensperger, U., ten Brink, H.M., 2004b. Artefacts in the sampling of nitrate studied in the "INTERCOMP" campaigns of EUROTRAC-AEROSOL. Atmos. Environ. 38, 6487-6496.

Schmidt, H., Derognat, C., Vautard, R., Beekmann, M., 2001. A comparison of simulated and observed ozone mixing ratios for the summer of 1998 in Western Europe. Atmospheric Envrionment 35, 6277-6297.

Seinfeld, J.H., Pandis, S.N., 1998. Atmospheric Chemistry and Physics, John Wiley, Hoboken, N.J.

Simpson, D., Fagerli, H., Jonson, J.E., Tsyro, S., Wind, P., Tuovinen, J.P., 2003. Transboundary Acidification and Eutrophication and Ground Level Ozone in Europe. Unified EMEP Model Description. Status Report 1, Part I.

Skamarock, W.C., Klemp, J.B., 2008. A time-split nonhydrostatic atmospheric model for weather research and forecasting applications. J. Comput. Phys., 227 (7), 3465-3485. doi: 10.1016/j.jcp.2007.01037.

Soret, A., Jiménez-Guerrero, P., Baldasano, J.M., 2011. Comprehensive air quality planning for the Barcelona Metropolitan Area through traffic management. Atmos. Poll. Res., 2, 255-266.

Stern, R., Builtjes, P., Schaap, M., Timmermans, T., Vautard, R., Hodzic, A., Memmesheimer, M., Feldmann, H., Renner, E., Wolke, R., Kerschbaumer, A., 2008. A model inter-comparision study focusing on episodes with elevated PM10 concentrations. Atmos. Environ., 42, 4567-4588.

Stockwell, W.R., Middleton, P., Chang, J.S., Tang, X., 1990. The second generation regional acid deposition model chemical mechanism for regional air quality modeling. J. Geophys. Res., 95, 16343-16367.

1000 Stockwell W.R., Kley, D., 1994. The Euro-RADM mechanism. A gas-phase chemical
1001 mechanism for European air quality studies, Beriche ds Forschungszentrums Jülich, 2868,
1002 Germany.

1003 Stockwell, W.R., Kirchner, F., Khun, M., Seefeld, S., 1997. A new mechanism for regional
1004 atmospheric chemistry modeling. J. Geophys. Res., 102, 25847-25879.

1005 Szopa, S., Foret, G., Menut, L., Cozic, A., 2009. Impact of large scale circulation on
1006 European summer surface ozone and consequences for modeling forecast. Atmos. Environ.,
1007 43, 1189-1195.

1008 Tarrasón, L., Iversen, T., 1998. Modelling intercontinental transport of atmospheric sulphur in
1009 the northern hemisphere, Telus B, 50, 4 331-352.

1010 Tarrasón, L., Fagerli, H., Klein, H., Simpson, D., Benedictow, A., Vestreng, V., Rigler, E,
1011 Emberson, L., Posh, M., Spranger, T., 2006. Transboundary acidification,eutrophication and
1012 ground level ozone in Europe from 1990 to 2004. Technical Report. EMEP Status Report
1013 1/06: to Support the Review of the Gothenburg Protocol. The Norwegian Meteorological
1014 Institute, Oslo, Norway.

1015 Tarrasón, L., Fagerli, H., Jonson, J.E.,Simpson, D., Benedictow, A. Klein, H.,Vestreng, V.,
1016 2007. Transboundary Acidification, Eutrophication and Ground Level Ozone in Europe in
1017 2005. EMEP Status Report 1/07. The Norwegian Meteorological Institute, Oslo, Norway.
1018 (Available at http://www.emep.int/publ/reports/2007/status_report_1_2007.pdf)

1019 Tesche, T.W., Morris, R., Tonnesen, G., McNally, D., Boylan, J., Brewer, P., 2006.
1020 CMAQ/CAMx annual 2002 performance evaluation over the eastern US. Atmos. Environ.,
1021 40, 4906-4919.

1022 Torseth, K., Hov. O., 2003. The EMEP monitoring strategy 2004-2009. Technical Report
1023 9/2003. EMEP/CCC.

1024 van Dingenen, R., Raes, F., Putaud, J.P., Baltensperger, U., Brüggemann, E., Charron, A.,
1025 Facchini, M.C., Decesari, S., Fuzzi, S., Gehrig, R., Hansson, H.C., Harrison, R.M., Hüglin,
1026 Ch., Jones, A.M., Laj, P., Lorbeer, G., Maenhaut, W., Palmgren, F., Querol, X., Rodríguez,
1027 S., Schneider, J., ten Brink, H., Tunved, P., Torseth, K., Wehner, B., Weingartner, E.,
1028 Wiedensohler, A., Wählin, P.A., 2004. European Aerosol Phenomenology I: Physical

1029 characteristics of particulate matter at kerbside, urban, rural and background sites in Europe.
1030 Atmos. Environ., 38, 2561-2577.

1031 van Loon, M., Roemer, M.G.M., Builtjes, P.J.H., Bessagnet, B., Rouïl, L., Christensen, J.,
1032 Brandt, J., Fegerli, H., Tarrasón, L., Rodgers, I., 2004. Model Inter-comparison in the
1033 framework of the review of the Unified EMEP model. TNO Report. Technical Report.
1034 R2004/282. 53pp.

1035 Vautard, R., Schaap, M., Bergström, R., Bessagnet, B., Brandt, J., Builtjes, P.J.H.,
1036 Christensen, J.H., Cuvelier, C., Foltescu, V., Graff, A., Kerschbaumer, A., Krol, M., Roberts,
1037 P., Rouïl, L., Stern, R., Tarrasón, L., Thunis, P., Vignati, E., Wind, P., 2009. Skill and
1038 uncertainty of a regional air quality model ensemble. Atmos. Environ., 43, 4822-4832.

1039 Vayenas, D.V., Takahama, S., Davidson, C.I., Pandis, S.N., 2005. Simulation of the
1040 thermodynamics and removal processes in the sulfate-ammonia-nitric acid system during
1041 winter: Implication for PM2.5 control strategies. J. Geophys. Res., 110 (D07S14),
1042 doi:10.1029/2004JD005038.

1043 Wu, S.-Y., Hu, J.-L., Zhang, Y., Aneja, V.P., 2008. Modeling atmospheric transport and fate
1044 of ammonia in North Carolina – Part II: effect of ammonia emissions of fine particulate
1045 matter formation. Atmos. Environ., 42, 3437-3451.

1046 Yarwood, G., Rao, S., Yocke, M., Whitten, G., 2005. Updates to the Carbon Bond Chemical
1047 Mechanism: CB05 Final Report to the US EPA, RT-0400676, available at:
1048 http://www.camx.com/publ/pdfs/BC05_Final_Report_120805.pdf.

1049 Yu, S., Dennis, R., Roselle, S., Nenes, A., Walker, J., Eder, B., Schere, K., Swall, J., Malm,
1050 W., Robarge, W., 2005. An assessment of the ability of three-dimensional air quality models
1051 with current thermodynamic equilibrium models to predict aerosol NO_3^-. J. Geophys. Res.,
1052 110, D07S13.

1053 Yu, S., Mathur, R., Sarwar, G., Kang, D., Tong, D., Pouliot, G, Pleim, J., 2010. Eta-CMAQ
1054 air quality forecasts for O_3 and related species using three different photochemical
1055 mechanisms (CB4, CB05, SAPRC-99): comparisons with measurements during the 2004
1056 ICARTT study. Atmos. Chem. Phys., 10, 3001-3025.

1057

Tables

Table 1: Total emission of SO_x, NO_x, NMVOC, PM2.5, PM coarse, CO and NH_3 for the year 2004 for anthropogenic activities in Europe sort by SNAP (Selected Nomenclature Air Pollution) category.

SNAP	Description	SO_x	NO_x	NMVOC	PM2.5	PM coarse	CO	NH_3
1	Energy transformation	9323	3483	137	295	386	852	7
2	Small combustion sources	1161	1028	1163	825	314	10803	7
3	Industrial combustion	2096	2096	180	299	202	5499	6
4	Industrial process	734	385	1504	552	315	3643	106
5	Extraction of fossil fuels	0	0	0	0	0	0	0
6	Solvent and product use	0	0	4300	21	11	22	5
7	Road transport	314	6491	4355	361	95	26001	82
8	Non road transport	2868	6166	754	487	57	3115	2
9	Waste handling and disposal	25	41	159	97	15	1832	143
10	Agriculture	2	246	508	176	332	535	5823
	Total	16522	19937	13059	3113	1727	52303	6182

Table 2. Coordinates, altitude and the chemical species measured of the 54 selected EMEP stations. The code is composed by 2-letter country code plus 2-digit station code. Zone is defined as follows: Western Iberian Peninsula (W.IP); Eastern Iberian Peninsula-Western Mediterranean (E.IP-W.Med), Central Mediterranean (C.Med), Eastern Mediterranean (E.Med), North of Italy (N. It.), Eastern Europe (E.Eu), Northwestern Europe (NW.Eu), Southern France (S.Fr.), Central Europe (C.Eu), Nordic (Nord), Central France (C.Fr) and North Atlantic (N.Atl).

	Station Name	Code	Zone	Lon.(º/N)	Lat.(º/E)	Alt.(m)	SO_4^{2-}	NO_3^-	NH_4^+	NH_3	HNO_3	TNH_3	TNO_3	SO_2
1	Anholt	DK08	Nord	56.717	11.517	40	x					x	x	x
2	Barcarrota	ES11	W.IP	38.476	-6.923	393	x	x				x	x	x
3	Birkenes	NO01	Nord	58.383	8.25	190	x	x	x	x	x	x	x	
4	Cabo de Creus	ES10	E.IP-W.Med	42.319	3.317	23	x	x				x	x	
5	Campisábalos	ES09	W.IP	41.281	-3.143	1360	x	x		x		x	x	x
6	Chopok	SK02	E.Eu	48.933	19.583	2008	x							
7	Deuselbach	DE04	NW.Eu	49.767	7.05	480	x					x	x	
8	Diabla Gora	PL05	E.Eu	54.15	22.067	157	x					x	x	
9	Donon	FR08	C.Eu	48.5	7.133	775	x							x
10	Els Torms	ES14	E.IP-W.Med	41.4	0.717	470	x	x				x	x	x
11	Eskdalemuir	GB02	NW.Eu	55.313	-3.204	243	x							
12	High Muffles	GB14	NW.Eu	54.334	-0.808	267	x							
13	Illmitz	AT02	E.Eu	47.767	16.767	117	x	x	x	x	x			x
14	Iraty	FR12	S.Fr	43.033	-1.083	1300	x							x
15	Iskrba	SI08	N.It	45.567	14.867	520	x					x	x	
16	Ispra	IT04	N.It	45.8	8.633	209	x	x	x					
17	Jarczew	PL02	E.Eu	51.817	21.983	180	x	x	x			x	x	x
18	Jungfraujoch	CH01	C.Eu	46.55	7.983	3573	x	x	x					
19	Kollumerwaard	NL09	NW.Eu	53.334	6.277	1		x	x					
20	Kosetice	CZ03	E.Eu	49.583	15.083	534	x					x	x	x
21	K-puszta	HU02	E.Eu	46.967	19.583	125	x	x	x	x	x			
22	La Tardière	FR15	C.Fr	46.65	0.75	746	x							
23	Le Casset	FR16	C.Eu	45	6.467	746	x							
24	Leba	PL04	Nord	54.75	17.533	2	x	x	x			x	x	x
25	Liesek	SK05	E.Eu	49.367	19.683	892	x	x			x			
26	Lough Navar	GB06	N.Atl	54.443	-7.87	126	x							
27	Melpitz	DE44	NW.Eu	52.53	12.93	86	x	x	x					
28	Montandon	FR14	C.Eu	47.183	6.5	746	x							
29	Montelibretti	IT01	C.Med	42.1	12.633	48	x	x	x	x	x			x
30	Morvan	FR10	C.Fr	47.267	4.083	620	x							
31	Niembro	ES08	W.IP	43.442	-4.85	134	x	x		x		x	x	x
32	O Savñao	ES16	W.IP	42.653	-7.705	506	x	x				x	x	x
33	Payerne	CH02	C.Eu	46.817	6.95	510	x					x	x	
34	Penausende	ES13	W.IP	41.283	-5.867	985	x	x				x	x	x
35	Peyrusse Vieille	FR13	S.Fr	43.375	0.104	236	x							x
36	Preila	LT15	Nord	55.35	21.067	5	x					x	x	x
37	Råö	SE14	Nord	57.4	11.917	5	x					x	x	
38	Revin	FR09	NW.Eu	49.9	4.633	390	x							x
39	Rigi	CH05	C.Eu	47.069	8.466	1030	x					x	x	x
40	Risco Llamo	ES15	W.IP	39.517	-4.35	1241	x	x				x	x	x
41	Rucava	LV10	Nord	56.217	21.217	5	x	x	x			x	x	x
42	Skreådalen	NO08	Nord	58.817	6.717	475	x	x	x	x	x	x	x	
43	Sniezka	PL03	E.Eu	50.733	15.733	1603	x	x	x			x	x	x
44	Starina	SK06	E.Eu	49.05	22.267	345	x	x			x			x
45	Svratouch	CZ01	E.Eu	49.733	16.033	737	x					x	x	x
46	Tange	DK03	Nord	56.35	9.6	13	x					x	x	x
47	Topolniky	SK07	E.Eu	47.96	17.861	113	x	x			x			
48	Utö	FI09	Nord	59.779	21.377	7	x		x			x	x	
49	Valentina Observatory	IE01	N.Atl	51.94	-10.244	11	x					x	x	
50	Vavihill	SE11	Nord	56.017	13.15	175	x					x	x	x
51	Víznar	ES07	E.IP-W.Med	37.233	-3.533	1265	x	x				x	x	
52	Yarner Wood	GB13	NW.Eu	50.596	-3.713	119	x							
53	Zarra	ES12	E.IP-W.Med	39.086	-1.102	885	x	x				x	x	x
54	Zoseni	LV16	Nord	57.133	25.917	183	x	x	x			x	x	x

1073 Table 3: Bias correlation coefficients of the secondary inorganic aerosol and their gas
1074 precursors between each other for all the data points available for 2004. Mean and standard
1075 deviation (STD) of the bias are in $\mu g\ m^{-3}$.

	NH_3	NO_3^-	HNO_3	SO_2	SO_4^{2-}	NH_4^+
Mean	-1.36	-1.01	-0.97	0.50	-0.29	-0.45
STD	1.09	2.10	1.64	2.14	1.31	1.08
NH_3	1.00 (7/2562)	0.03 (7/2562)	0.55 (5/1830)	-0.03 (4/1464)	0.02 (7/2562)	0.07 (5/1830)
NO_3^-		1.00 (27/9882)	-0.16 (8/2928)	-0.06 (15/5490)	0.29 (26/9516)	0.75 (14/5124)
HNO_3			1.00 (8/2928)	-0.07 (3/1098)	0.04 (8/2928)	0.00 (5/1830)
SO_2				1.00 (31/11346)	0.01 (25/9150)	0.07 (7/2562)
SO_4^{2-}					1.00 (53/19398)	0.59 (14/5124)
NH_4^+						1.00 (15/5490)

1076 [a]Value reported without parenthesis represents the correlation coefficient.
1077 [b]The first and second values in parenthesis represent the number of stations and the number of
1078 data points respectively used to calculate the correlation coefficient.

1079

Table 4: List of published European model evaluation studies for secondary inorganic aerosol and their main characteristics to be compared with CALIOPE-EU evaluation results (this study).

Reference	Modeled Year[1]	Modeling System	Horizontal Resolution/layers	Chemical Mechanism[2]	Thermodynamic Inorganic Equilibrium[3]	Study number
This study	2004	CALIOPE	12 km x 12 km/15	CBM-IV	ISORROPIA	CALIOPE-EU04
Kim et al. (2011)	2001	POLYPHEMUS	0.5º x 0.5º/5	RACM	ISORROPIA	POLYPHEMUS1
Kim et al. (2011)	2001	POLYPHEMUS	0.5º x 0.5º/5	CB05	ISORROPIA	POLYPHEMUS2
Matthias (2008)	2001	CMAQ	54 km x 54 km/20	CBM-IV	ISORROPIA	CMAQ3
Stern et al. (2008)	2003	CHIMERE	0.25 º x 0.25 º/8	MELCHIOR	ISORROPIA	CHIMERE4
Stern et al. (2008)	2003	EURAD	125 km x 125 km/23	EuroRADM	RPMARES	EURAD4
Stern et al. (2008)	2003	LOTOS-EUROS	0.25º x 0.25º/4	CBM-IV	ISORROPIA	LOTOS-EUROS4
Stern et al. (2008)	2003	REM-CALGRID	0.25º x 0.25º/5	CBM-IV	ISORROPIA	REM-CALGRID4
Stern et al. (2008)	2003	LM-MUSCAT	0.25º x 0.25º/40	RACM	Hinneburg et al. (2007)	LM-MUSCAT4
Sartelet et al. (2007)	2001	POLYPHEMUS	0.5º x 0.5º/5	RACM	ISORROPIA	POLYPHEMUS5
Tarrasón et al. (2006)	2004	Unified EMEP	50 km x 50 km/20	EMEP	EQSAM	EMEP6
van Loon et al. (2004)	1999/2001	CHIMERE	0.5º x 0.5º/8	MELCHIOR	ISORROPIA	CHIMERE7
van Loon et al. (2004)	1999/2001	DEHM	50 km x 50 km/20	EMEP	EQSAM	DEHM7
van Loon et al. (2004)	1999/2001	Unified EMEP	50 km x 50 km/10	EMEP	EQSAM	EMEP7
van Loon et al. (2004)	1999/2001	MATCH	55 km x 55 km/10	EMEP	EQSAM	MATCH7
van Loon et al. (2004)	1999/2001	LOTOS	0.25º x 0.5º/3	CBM-IV	ISORROPIA	LOTOS7
van Loon et al. (2004)	1999/2001	CMAQ	36 km x 36 km/21	RADM2	ISORROPIA	CMAQ7
van Loon et al. (2004)	1999/2001	REM-CALGRID	0.25º x 0.5º	CBM-IV	ISORROPIA	REM-CALGRID7
Schaap et al. (2004)	1995	LOTOS	25 km x 25 km/3	CBM-IV	ISORROPIA	LOTOS8
Hass et al. (2003)	1995	DEHM	50 km x 50 km/10	CBM-IV	EQSAM	DEHM9
Hass et al. (2003)	1995	EURAD	27 km x 27 km/15	EuroRADM	RPMARES	EURAD9
Hass et al. (2003)	1995	EUROS	0.55º x 0.55º/4	CBM-IV	EQSAM	EUROS9
Hass et al. (2003)	1995	LOTOS	0.25º x 0.5º/3	CBM-IV	ISORROPIA	LOTOS9
Hass et al. (2003)	1995	MATCH	55 km x 55 km/10	EMEP	EQSAM	MATCH9
Hass et al. (2003)	1995	REM-CALGRID	0.25º x 0.5º	CBM-IV	ISORROPIA	REM-CALGRID9

[1]Evaluation studies are done over a full year. Evaluated period for Kim et al (2001) corresponds from 15 July to 15 August. Evaluated period for Stern et al. (2008) corresponds from 6 February to 30 March.

[2]CBM-IV, see Gery et al. (1989); CB05, see Yarwood et al. (2005); EMEP, see Simpson et al. (2003); EuroRADM, see Stockwell and Kley (1994); MELCHIOR, see Schmidt et al. (2001); RACM, see Stockwell et al. (1997); RADM2, see Stockwell et al. (1990).

[3]ISORROPIA, see Nenes et al. (1998); RPMARES, see Binkowski and Shankar (1995); EQSAM, see (Metzger et al., 2002).

Table 5: Comparison of the statistics modeled mean/observed mean (Ratio), correlation coefficient (r), and root mean squared error (RMSE, μg m^{-3}) between CALIOPE-EU and other European models[1,2] for secondary inorganic aerosol (SO_4^{2-}, NO_3^-, and NH_4^+) in daily basis.

Study Number	SO_4^{2-} daily average			NO_3^- daily average			NH_4^+ daily average		
	Ratio	r	RMSE	Ratio	r	RMSE	Ratio	r	RMSE
CALIOPE-EU04	0.82 (0.56,2.0)	0.49 (0.15,0.81)	1.30 (0.3,2.3)	0.50 (0.14,2.0)	0.58 (0.20,0.77)	2.30 (0.6,3.8)	0.67 (0.38,1.35)	0.62 (0.30,0.73)	1.20 (0.3,4.1)
POLYPHEMUS1	0.86			1.5			1.1		
POLYPHEMUS2	0.96			1.7			1.2		
CMAQ3	0.83 (0.54,1.36)	(0.21,0.72)		0.62 (0.39,1.0)	(0.30,0.80)		0.75 (0.53,0.94)	(0.30,0.75)	
CHIMERE4	0.69	0.48	3.4						
EURAD4	0.64	0.46	3.3						
LOTOS-EUROS4	0.57	0.47	3.7						
REM-CALGRID4	0.99	0.47	2.9						
LM-MUSCAT4	0.91	0.57	2.7						
POLYPHEMUS5	0.84	0.56	1.7	1.6	0.41	3.1	1.1	0.52	1.3
EMEP6	0.86	0.67		1.4	0.80		1.2	0.82	
CHIMERE7	0.67/0.72	0.49/0.53	2.5/2.07	0.94/0.80	0.44/0.46	2.74/2.73	1.11/1.01	0.41/0.56	1.27/1.38
DEHM7	0.93/0.85	0.57/0.55	2.36/1.77	1.80/1.63	0.34/0.25	3.02/2.53	1.10/0.79	0.51/0.49	0.98/0.83
EMEP7	0.91/0.88	0.57/0.58	2.1/1.84	1.63/1.04	0.50/0.34	3.51/2.08	1.26/1.00	0.51/0.47	1.22/0.86
MATCH7	1.0/1.17	0.56/0.62	2.1/1.86	0.88/0.83	0.47/0.40	1.74/1.59	1.01/1.62	0.53/0.55	0.94/2.09
LOTOS7	1.03/1.3	0.37/0.50	2.9/2.89	0.79/0.95	0.26/0.17	2.19/1.94	1.21/1.01	0.37/0.44	1.21/1.10
CMAQ7	1.22/-	0.46/-	2.67/-	2.65/-	0.47/-	1.74/-	-/-	-/-	-/-
REM-CALGRID7	0.91/0.93	0.51/0.53	2.36/2.03	1.15/0.74	0.42/0.35	2.43/1.92	1.33/1.23	0.45/0.45	1.24/0.99
LOTOS8	0.92	0.60	2.60	1.10	0.58	3.57	1.08	0.62	1.54
DEHM9	1.11	0.37	5.89	1.07	0.32	4.12	0.94	0.39	2.43
EURAD9	1.52	0.52	4.25	2.04	0.61	6.14	1.87	0.50	2.90
EUROS9	0.98	0.47	4.39	2.13	0.30	6.39	-	-	-
LOTOS9	0.91	0.54	2.76	1.59	0.49	4.07	1.23	0.51	1.57
MATCH9	0.84	0.65	2.49	0.78	0.50	2.55	0.55	0.61	1.46
REM-CALGRID9	0.81	0.50	2.78	1.07	0.53	3.10	1.07	0.43	1.63

[1]Value reported without parenthesis represents yearly averages in the entire domain. The first and second values in parenthesis represent the minimum and maximum value respectively obtained among all stations in the entire domain. [2]Values reported with a slash correspond to two different years studied: the number before the slash corresponds to the year 1999; the number after the slash correspond to the year 2001.

1100 Table 6: Comparison of the statistics modeled mean/observed mean (Ratio), correlation
1101 coefficient (r), and root mean squared error (RMSE, μg m^{-3}) between CALIOPE-EU and
1102 other European models[1,2] for total nitrate (TNO_3 = HNO_3+NO_3^-), total ammonia
1103 (TNH_3=NH_3+NH_4^+) and gas-phase aerosol precursors (HNO_3 and NH_3) in daily basis. Note
1104 that the other gas-phase aerosol precursors, SO_2 and NO_2 have been compared with other
1105 European studies in Pay et al. (2010a).

1106

1107

Study Number	HNO_3 daily average			TNO_3 daily average			NH_3 daily average			TNH_3 daily average		
	Ratio	r	RMSE	Ratio	r	RMSE	Ratio	r	RMSE	Ratio	r	RMSE
CALIOPE-EU04	1.00 (0.35,4.0)	0.41 (-0.11,0.78)	1.1 (0.4,3.5)	0.77 (0.45,1.2)	0.50 (0.14,0.70)	2.1 (0.9,3.6)	0.71 (0.1,1.0)	0.56 (0.10,0.40)	1.1 (0.3,1.3)	0.94 (0.62,2)	0.50 (0.10,0.72)	1.8 (0.4,3.3)
CHIMERE4				0.70	0.47	4.4				1.1	0.49	1.9
EURAD4				2.90	0.46	19.4				3.0	0.45	8.3
LOTOS-EUROS4				0.94	0.67	3.1				1.0	0.58	1.6
REM-CALGRID4				0.87	0.56	3.5				1.4	0.57	2.1
LM-MUSCAT4				0.44	0.42	5.8				1.6	0.56	3.5
POLYPHEMUS5	1.85	0.26	1.4				0.85	0.29	5.4			
EMEP6	0.73	0.38		1.23	0.87					1.26	0.63	
CHIMERE7				0.90/0.83	0.39/0.37	3.02/2.82				1.18/1.05	0.35/0.43	2.98/1.74
DEHM7				1.68/1.73	0.42/0.31	3.03/3.02				0.86/0.79	0.46/0.45	1.85/1.14
EMEP7				1.40/1.16	0.51/0.36	2.62/2.42				1.05/1.00	0.42/0.40	1.95/1.28
MATCH7				0.85/0.95	0.52/0.41	1.88/1.91				0.71/1.62	0.48/0.42	1.82/2.17
LOTOS7				0.72/0.70	0.23/0.20	2.31/2.27				1.12/1.01	0.27/0.29	2.25/1.49
CMAQ7				1.82/-	0.52/-	1.88/-				-/-	-/-	-/-
REM-CALGRID7				1.10/0.86	0.39/0.31	2.26/3.02				1.35/1.23	0.27/0.30	2.39/1.49
LOTOS8				0.81	0.52	2.31				0.88	0.58	1.50
DEHM9				1.09	0.45	2.75	0.38	0.27	7.38	0.79	0.47	3.69
EURAD9				1.85	0.50	3.72	0.56	0.15	5.88	1.24	0.54	3.40
EUROS9				2.49	0.41	5.17	-	-	-	-	-	-
LOTOS9				1.67	0.44	2.82	0.18	0.05	7.50	0.58	0.46	2.77
MATCH9				0.94	0.52	1.94	0.64	0.33	5.59	0.84	0.57	2.54
REM-CALGRID9				1.20	0.38	2.13	0.58	0.09	6.10	0.91	0.26	3.09

[1]Value reported without parenthesis represents yearly averages in the entire domain. The first and second values in parenthesis represent the minimum and maximum value respectively obtained among all stations in the entire domain. [2]Values reported with a slash correspond to two different years studied: the number before the slash corresponds to the year 1999; the number after the slash correspond to the year 2001.

Figures

Figure 1: Distribution of the emission (Mg/yr) of NH_3 (a), SO_x (b), NO_x (c), NMVOC (d).

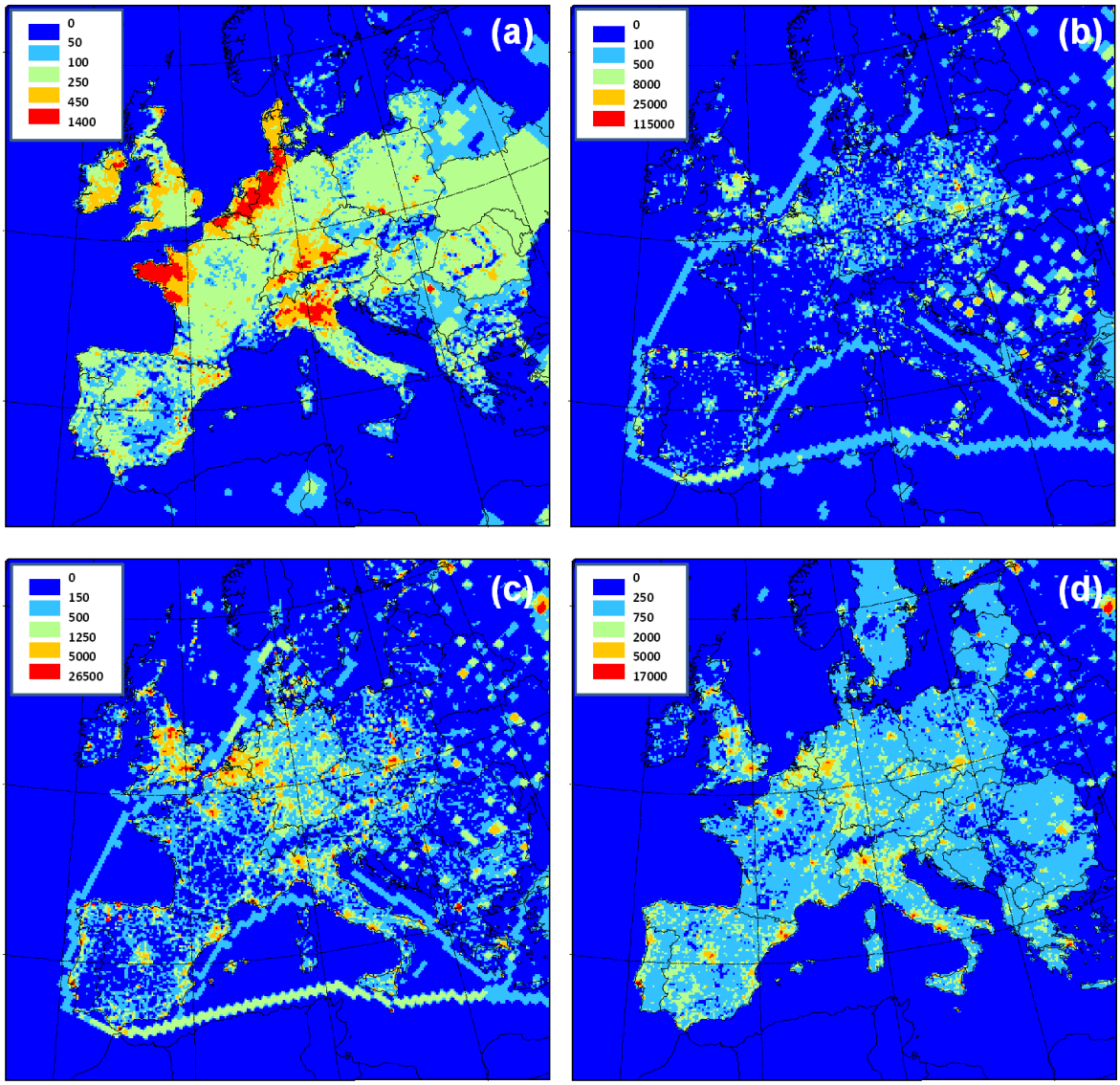

Figure 2: Spatial distribution of 54 selected EMEP stations over the study domain. The different colors indicate the different zones defined in Table 2. Number of each station is listed in Tables 2.

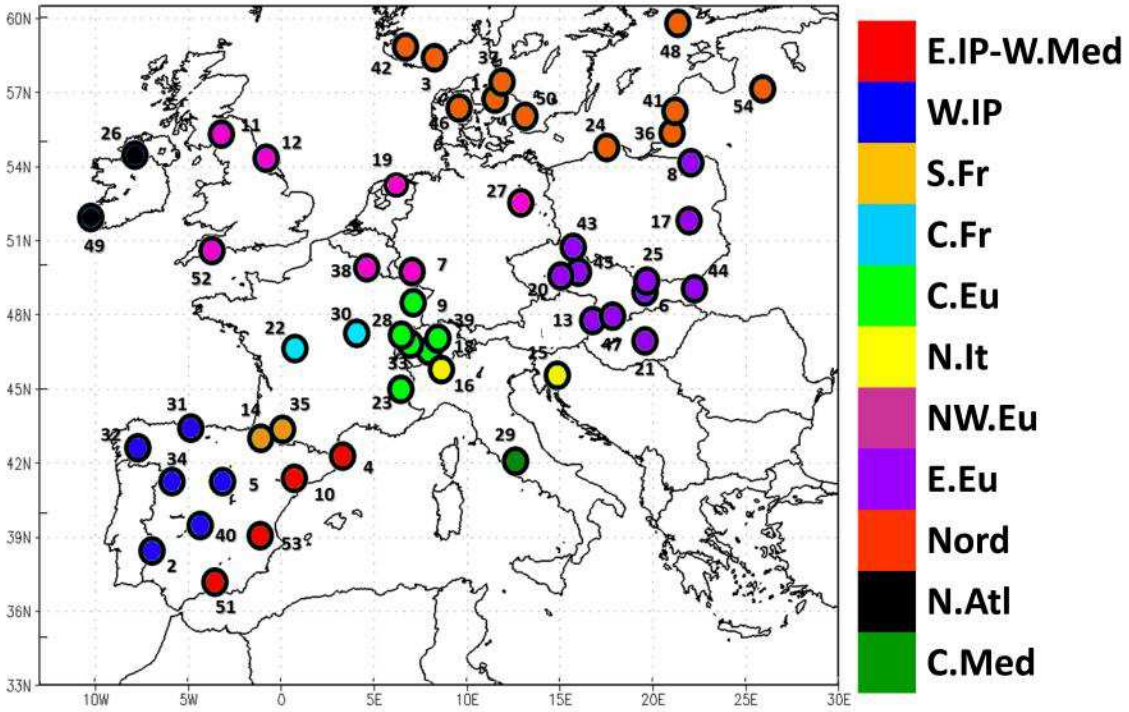

Figure 3: Annual temporal series for SO_2 (a), fine-particle SO_4^{2-} (b), HNO_3 (c), fine-particle NO_3^- (d), gas-phase NH_3 (e), fine-particle NH_4^+ (f), TNO_3 (g) and TNH_4^+ (h) in daily basis calculated as an average over all EMEP stations in 2004. Diamonds represent EMEP measurements (in µg m^{-3}) and black continuous lines represent CALIOPE-EU outputs (in µg m^{-3}). Blue columns indicate daily mean bias (µg m^{-3}). Annual statistics are shown top-right: observed mean (OM), modeled mean (MM), number of data points (N), correlation coefficient (r) and root mean squared error (RMSE).

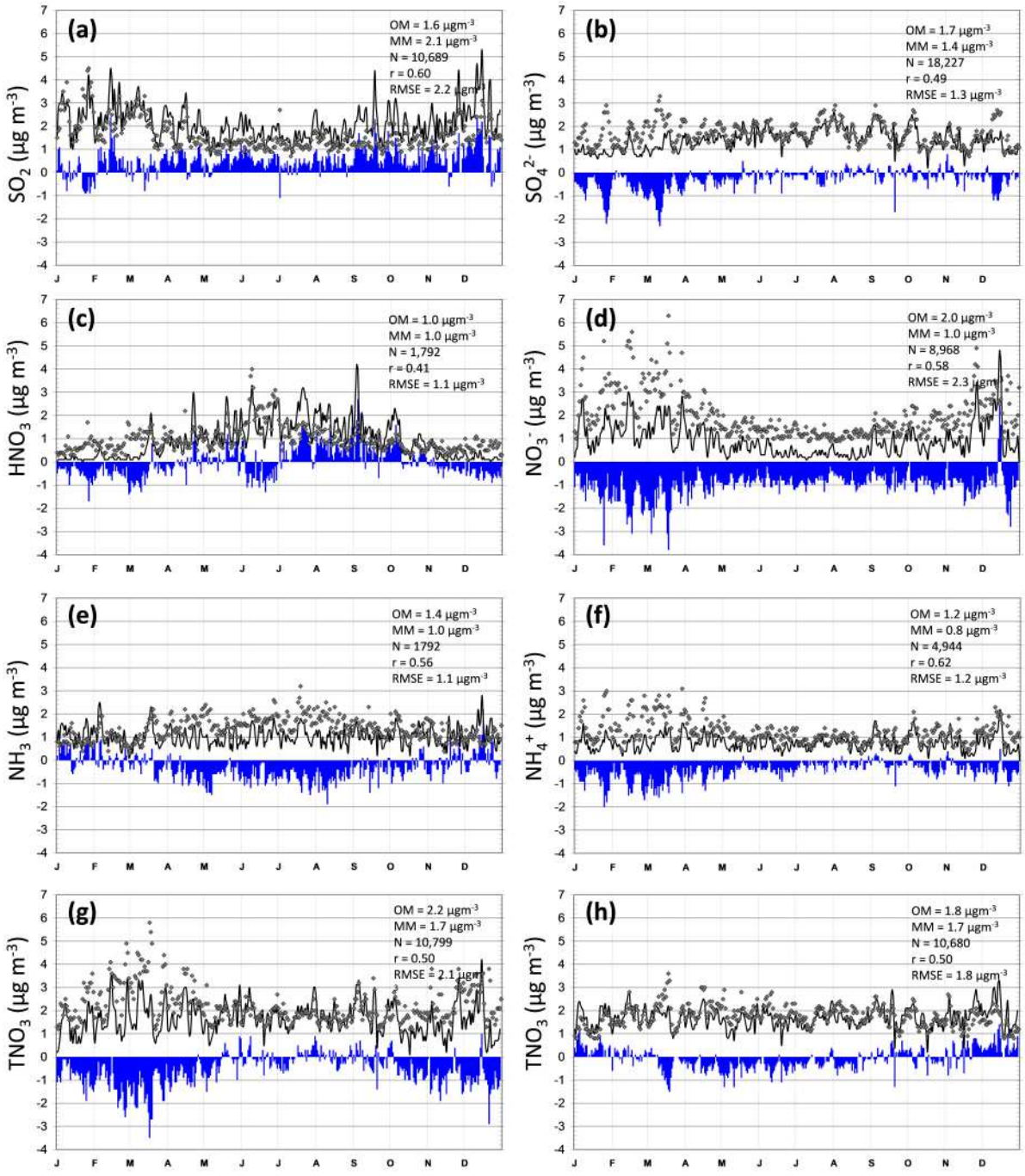

Figure 4: Monthly mean fractional bias (MFB, right column), and mean fractional error (MFE, left column) compared with goals and criteria proposed by Boyland and Rusell (2006). MFB and MFE are averaged over the sites within the EMEP network in 2004 for: SO_2 and SO_4^{2-} (a and b); HNO_3, NO_3^- and TNO_3 (c and d); and NH_3, NH_4^+ and TNH_3 (e and f). Dotted lines represent the goals (MFB $\leq \pm$ 30 % and MFE $\leq$ 50%). Broken lines represent the criteria (MFB $\leq \pm$ 60 % and MFE $\leq$ 75%).

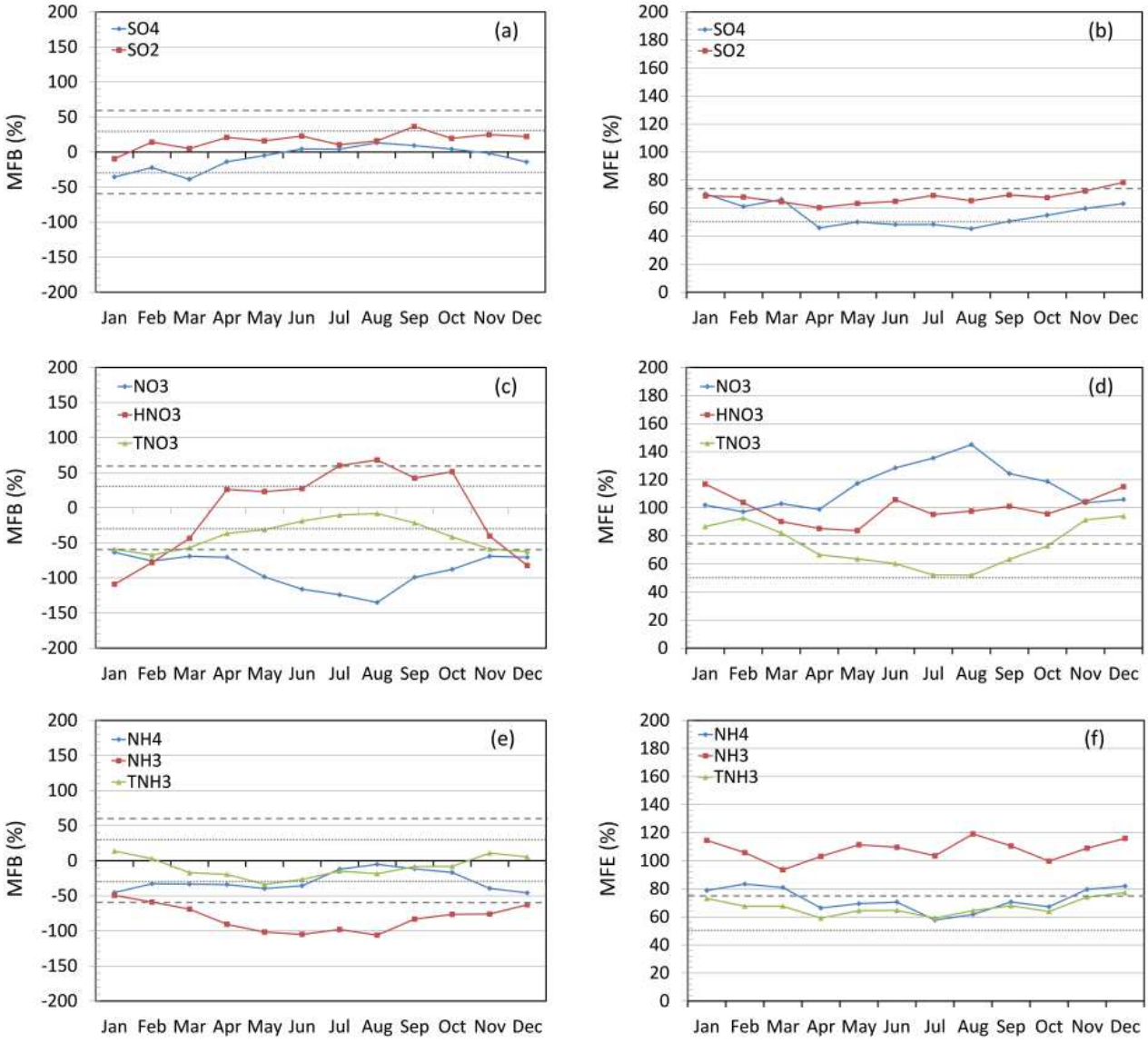

Figure 5: 2004 annual mean distributions over Europe for SO_2 (a), fine-particle SO_4^{2-} (b), HNO_3 (c), fine-particle NO_3^- (d), gas-phase NH_3 (e), fine-particle NH_4^+ (f), TNO_3 (g) and TNH_4^+ (h) at the lowest level. Points represent measured annual concentrations at the EMEP stations. Number at bottom-left in each figure is the spatial correlation between modeled and observed annual mean at each station.

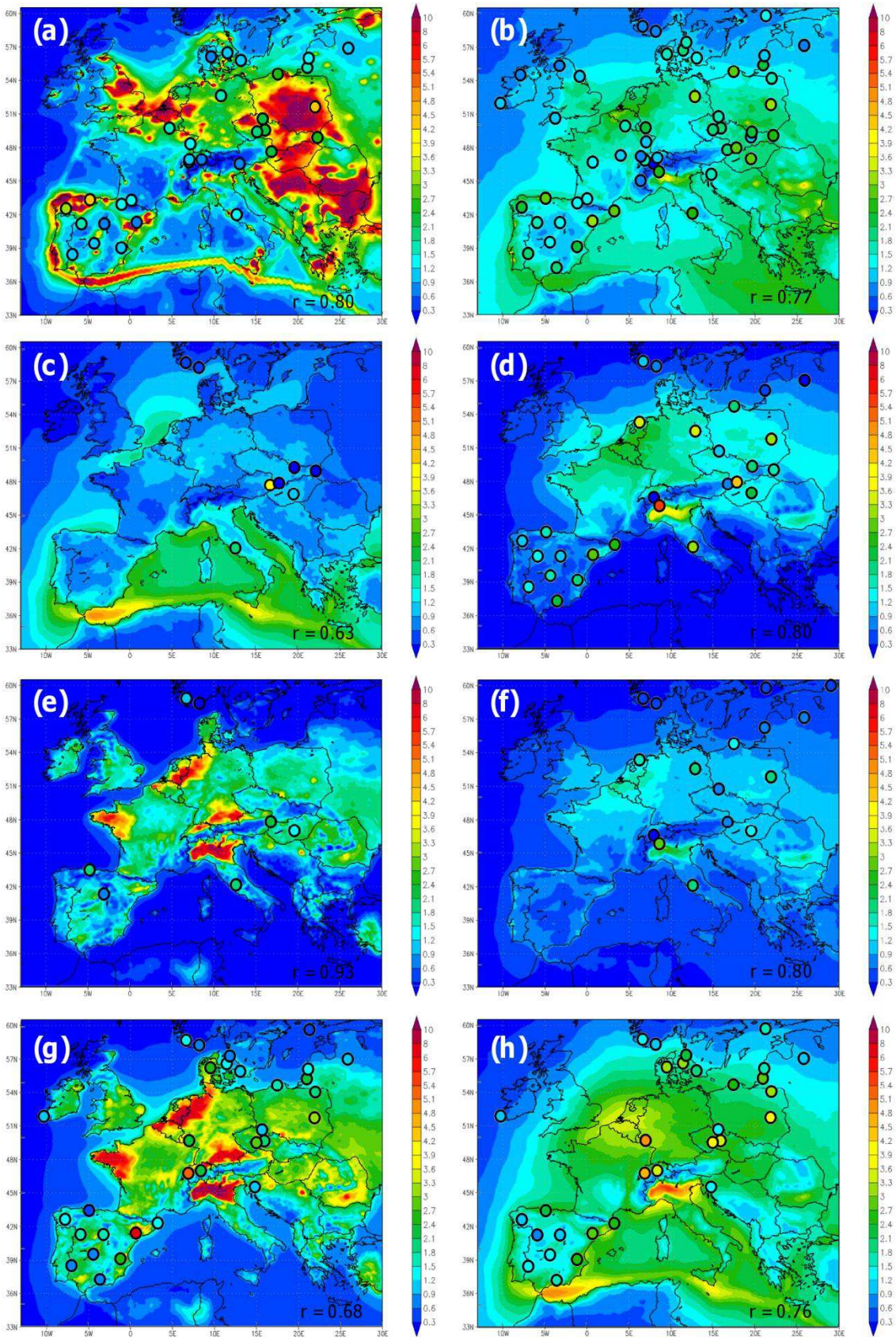

1143

Figure 6: Annual spatial distribution of the indicators: S-ratio (a and b), Free ammonia (c and d, in molar basin), and G-ratio (e and f) calculated within the CALIOPE-EU system over Europe in 2004. Dots represent the estimated indicators based on EMEP measurements.

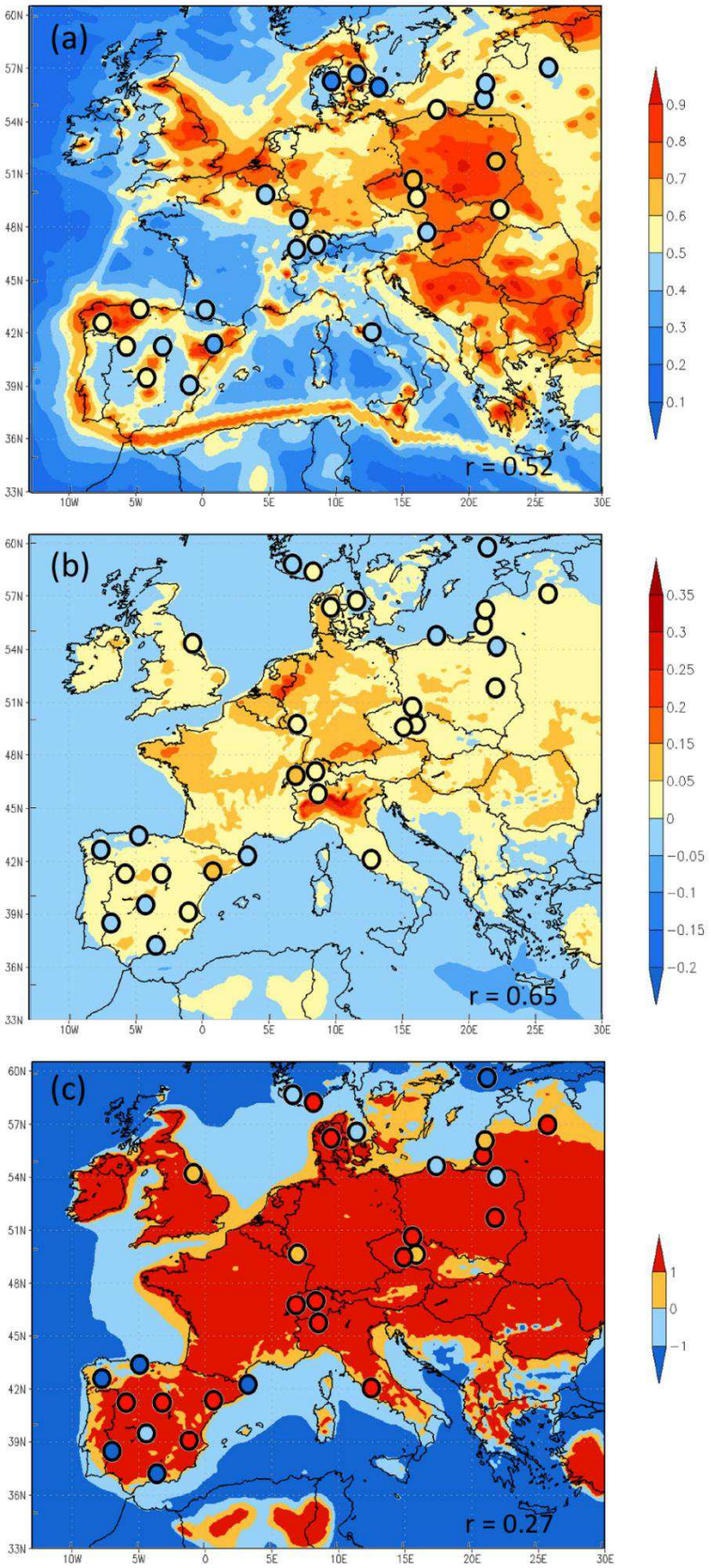
(a)
r = 0.52
(b)
r = 0.65
(c)
r = 0.27
60N
57N
54N
51N
48N
45N
42N
39N
36N
33N
10W
5W
0
5E
10E
15E
20E
25E
30E
0.9
0.8
0.7
0.6
0.5
0.4
0.3
0.2
0.1
0.35
0.3
0.25
0.2
0.15
0.05
0
−0.05
−0.1
−0.15
−0.2
1
0
−1

1147

Figure 7: Modeled and observed annual (a) SO_2 concentrations ($\mu g\ m^{-3}$), (b) SO_4^{2-} concentrations, and (c) S-ratio defined as $SO_2/(SO_2+SO_4^{2-})$ for each EMEP stations. The observed values are the light grey columns and the modeled values are the dark grey column. EMEP stations are represented by a code defined in Table 2 and they are sorted according to zones described in Table 2.

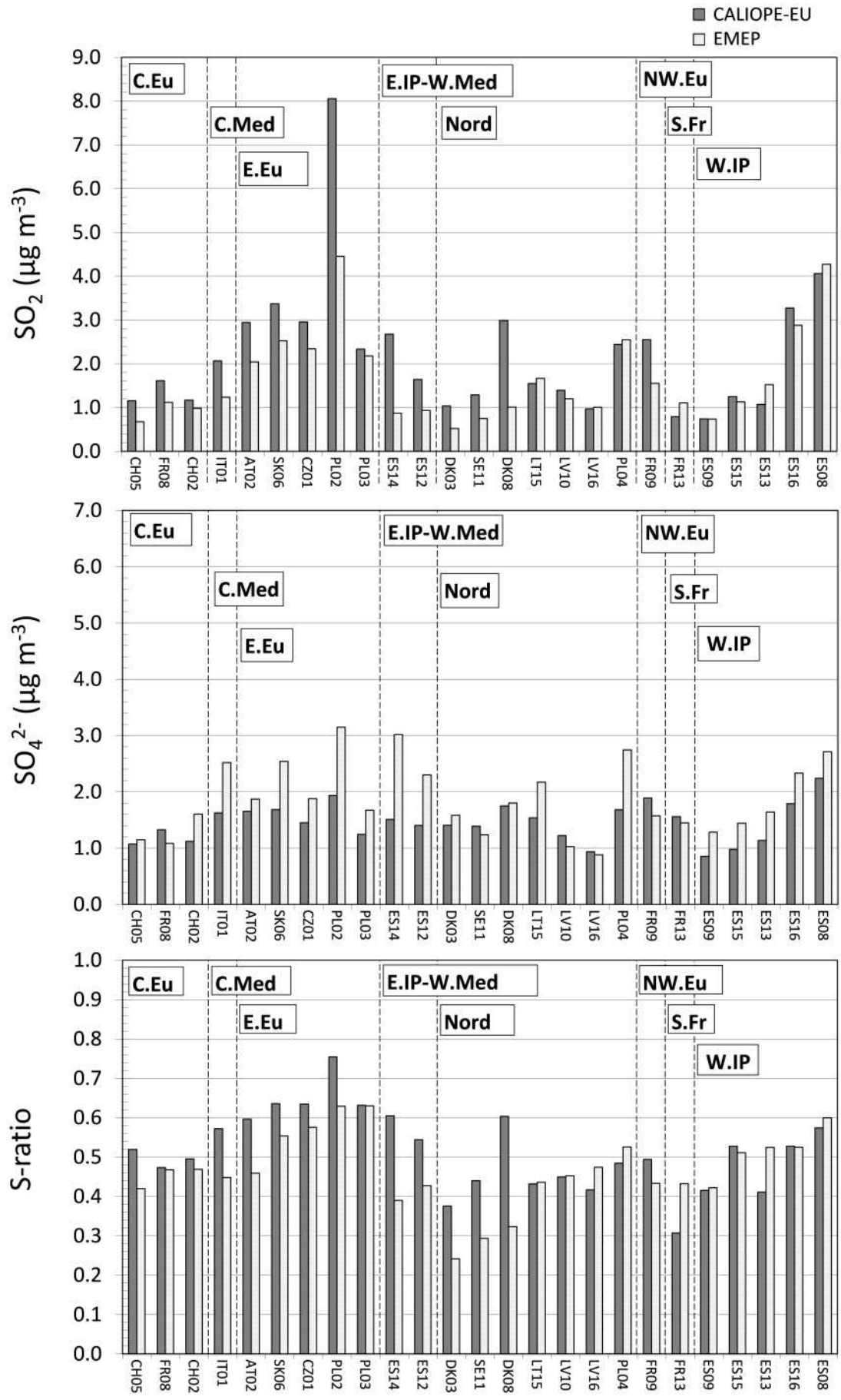
CALIOPE-EU
EMEP
SO_2 (µg m^{-3})
SO_4^{2-} (µg m^{-3})
S-ratio
C.Eu
C.Med
E.Eu
E.IP-W.Med
Nord
NW.Eu
S.Fr
W.IP
CH05 FR08 CH02 IT01 AT02 SK06 CZ01 PL02 PL03 ES14 ES12 DK03 SE11 DK08 LT15 LV10 LV16 PL04 FR09 FR13 ES09 ES15 ES13 ES16 ES08

1153

Figure 8: Modeled and observed annual (a) Free ammonia ($F\text{-}NH_x$, µmol m^{-3}), (b) Total nitrate (TNO_3, µg m^{-3}), and (c) G-ratio defined as $F\text{-}NH_x$ over TNO_3 on molar basis. The observed values are the light grey columns and the modeled values are the dark grey column. EMEP stations are represented by a code defined in Table 2 and they are sorted according to zones described in Table 2.

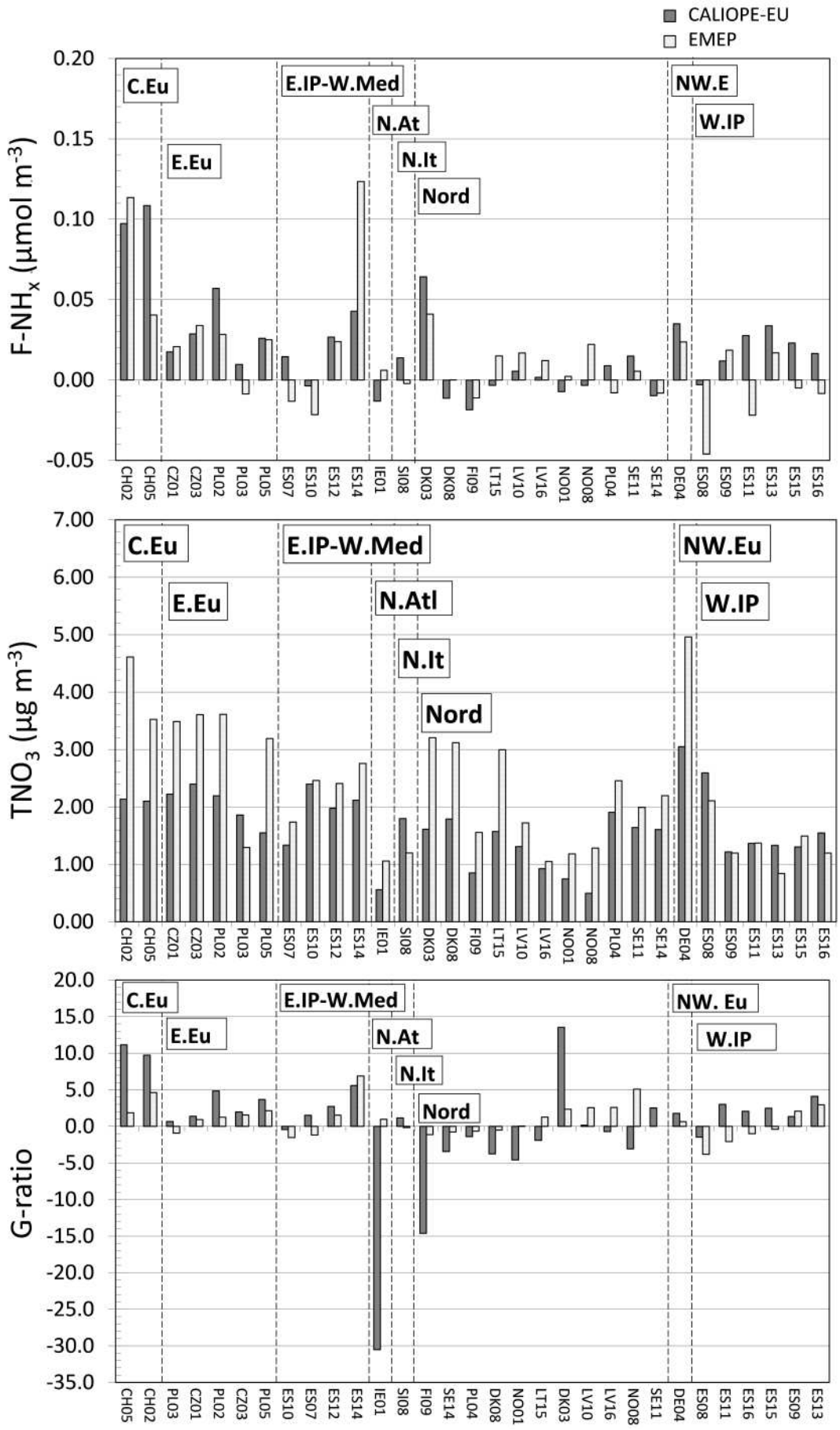
CALIOPE-EU
EMEP
F-NHx (µmol m-3)
C.Eu
E.Eu
E.IP-W.Med
N.At
N.It
Nord
NW.E
W.IP
CH02 CH05 CZ01 CZ03 PL02 PL03 PL05 ES07 ES10 ES12 ES14 IE01 SI08 DK03 DK08 FI09 LT15 LV10 LV16 NO01 NO08 PL04 SE11 SE14 DE04 ES08 ES09 ES11 ES13 ES15 ES16
TNO3 (µg m-3)
C.Eu
E.Eu
E.IP-W.Med
N.Atl
N.It
Nord
NW.Eu
W.IP
CH02 CH05 CZ01 CZ03 PL02 PL03 PL05 ES07 ES10 ES12 ES14 IE01 SI08 DK03 DK08 FI09 LT15 LV10 LV16 NO01 NO08 PL04 SE11 SE14 DE04 ES08 ES09 ES11 ES13 ES15 ES16
G-ratio
C.Eu
E.Eu
E.IP-W.Med
N.At
N.It
Nord
NW. Eu
W.IP
CH05 CH02 PL03 CZ01 PL02 CZ03 PL05 ES10 ES07 ES12 ES14 IE01 SI08 FI09 SE14 PL04 DK08 NO01 LT15 DK03 LV10 LV16 NO08 SE11 DE04 ES08 ES11 ES16 ES15 ES09 ES13

1159

SUPPLEMENTARY MATERIAL

1. Annual pattern for NO_2

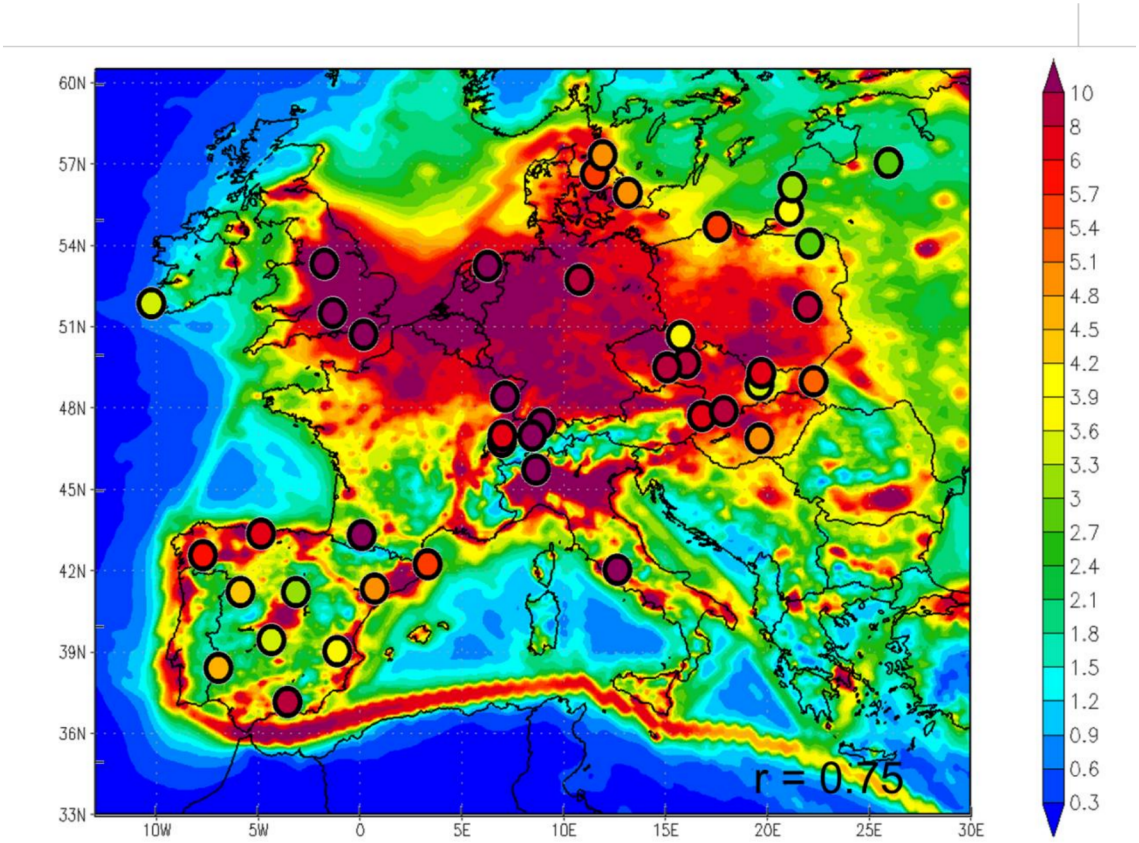

Figure S1: Annual average concentrations (in μg m^{-3}) for NO_2 at lower-most level simulated by CALIOPE over Europe at a 12 km x 12 km spatial resolution in 2004. Points represent measured annual concentrations at the EMEP stations. Number at bottom-left in each figure is the spatial correlation between modeled and observed annual mean at each station.

Figure1

Click here to download high resolution image

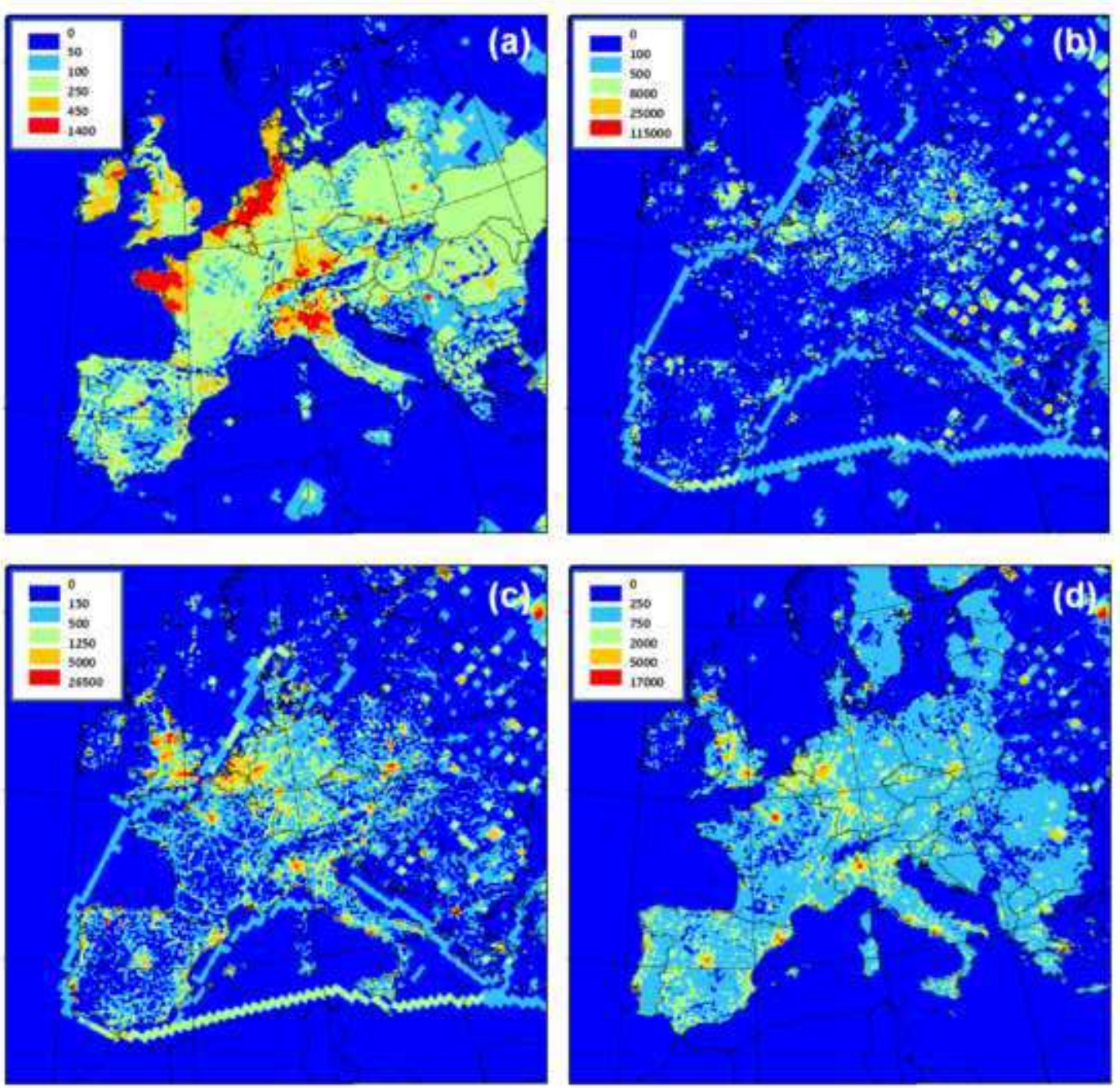

Figure2

Click here to download high resolution image

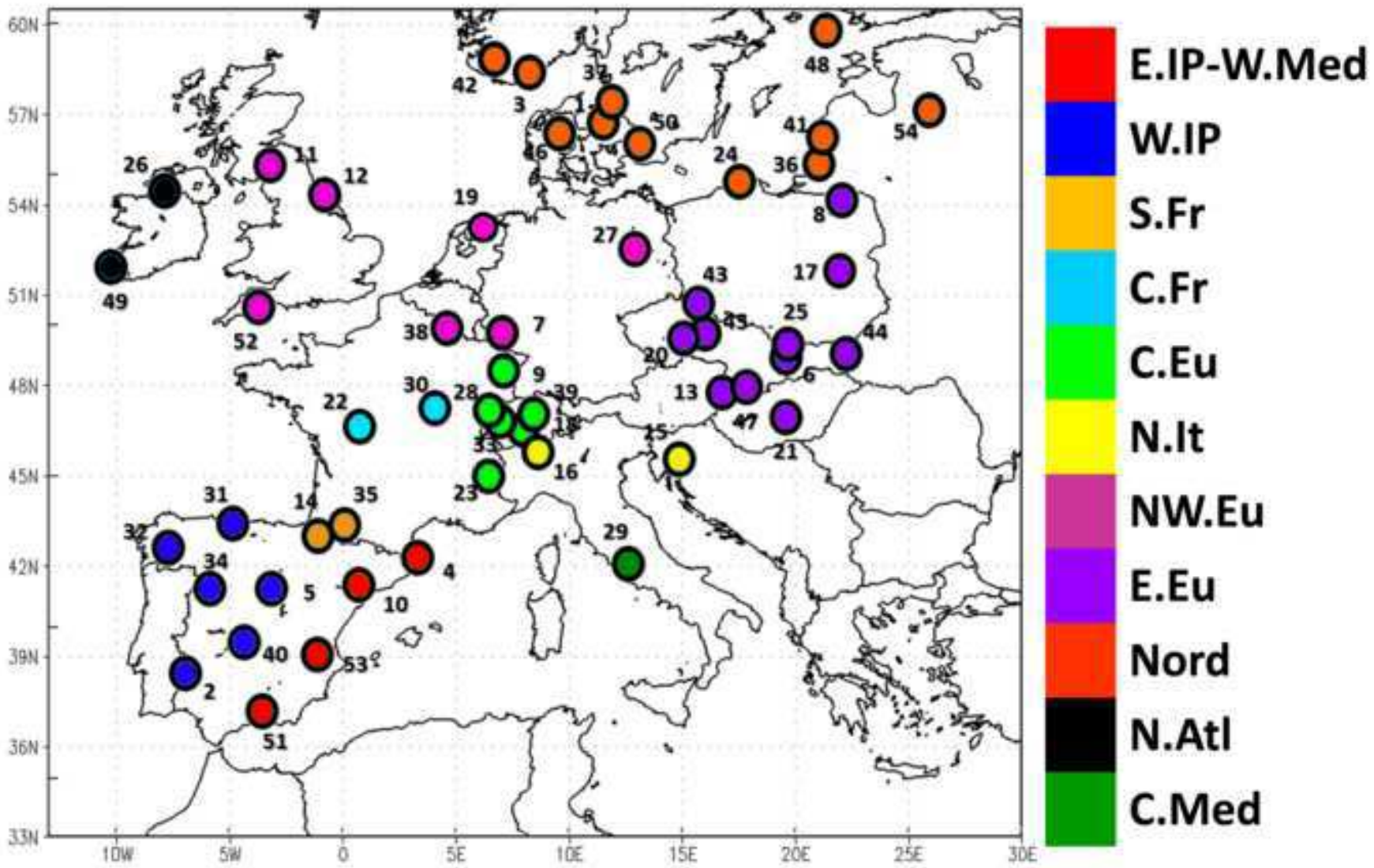

Figure3

Click here to download high resolution image

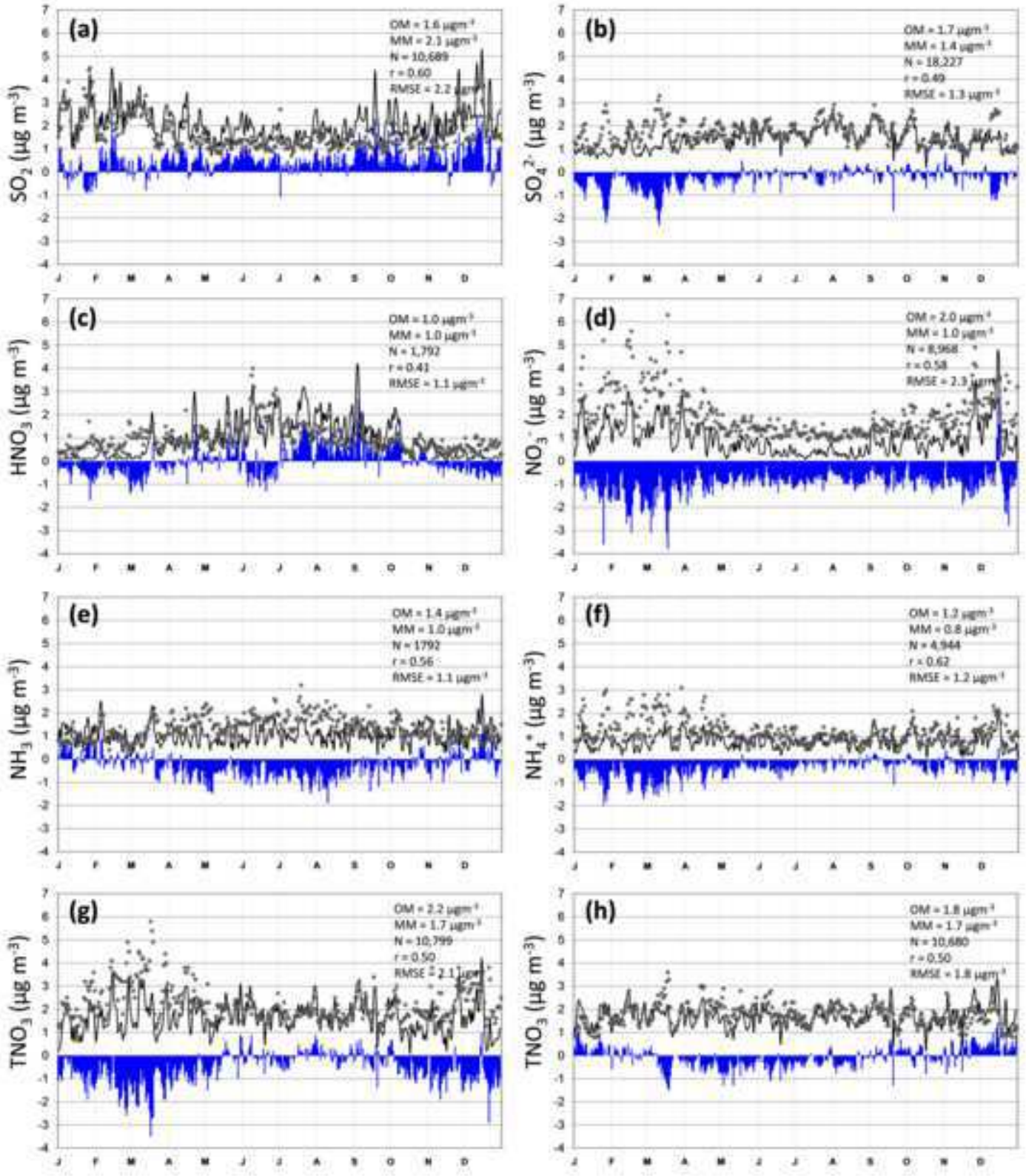

Figure4

Click here to download high resolution image

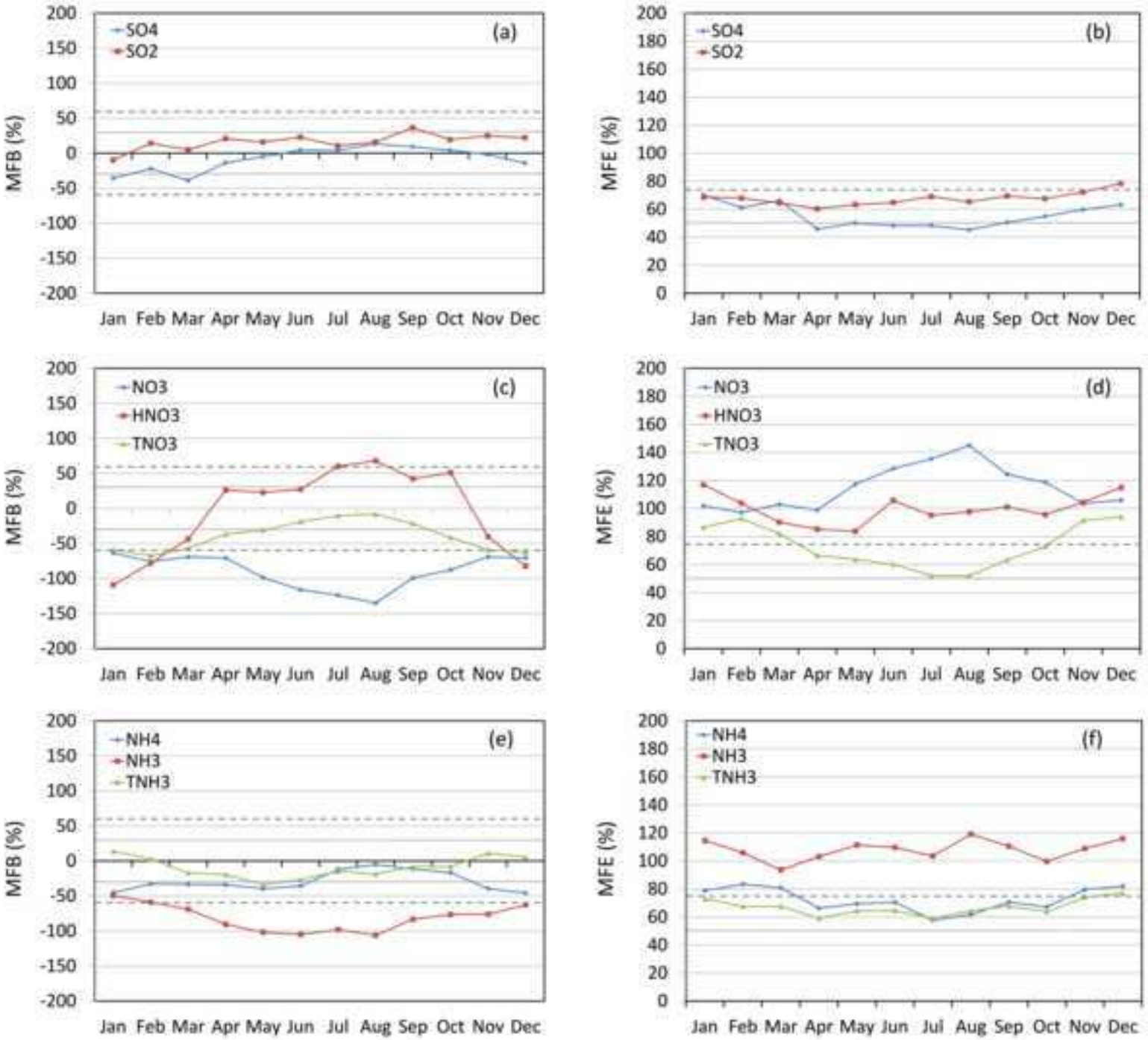

Figure5

Click here to download high resolution image

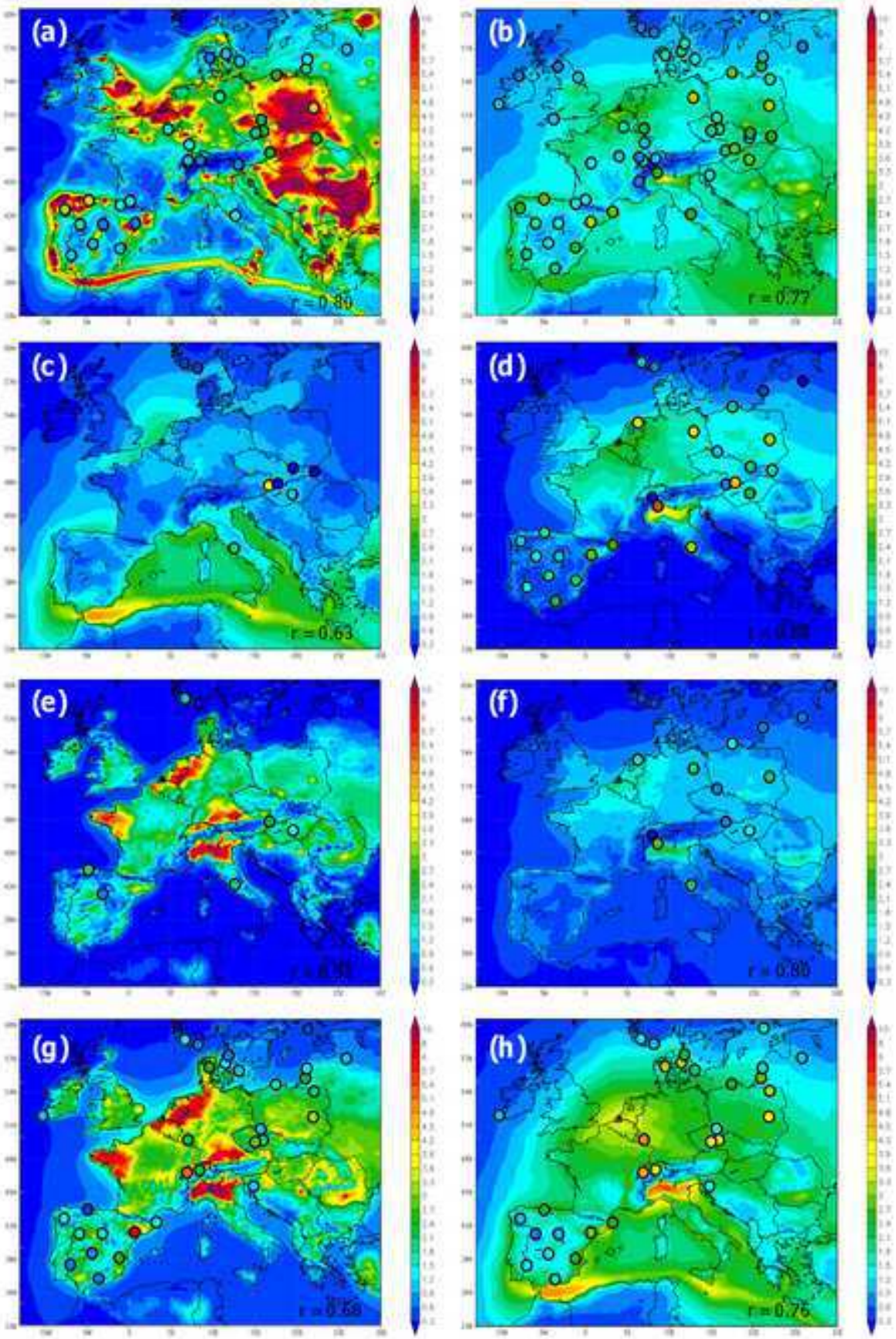

Figure6

Click here to download high resolution image

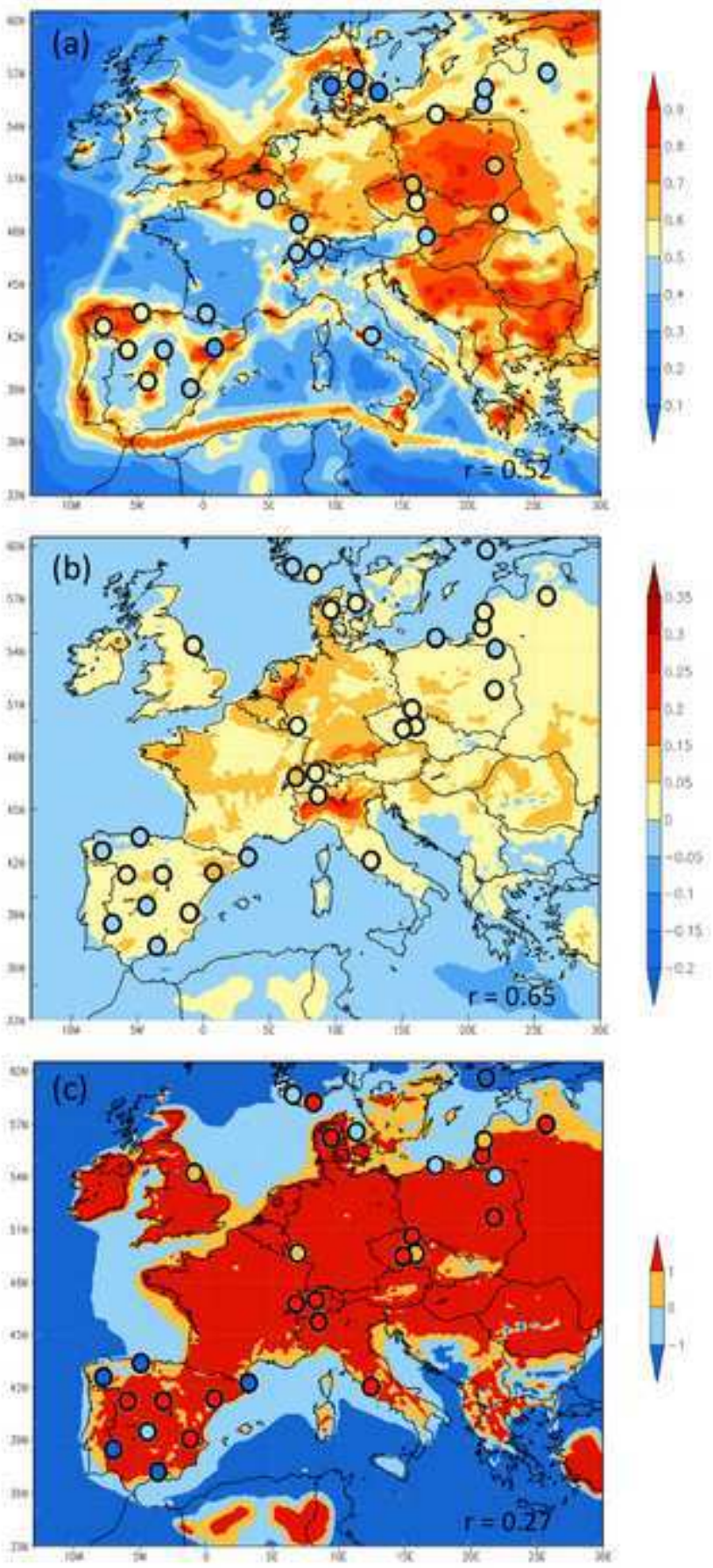

Figure7

Click here to download high resolution image

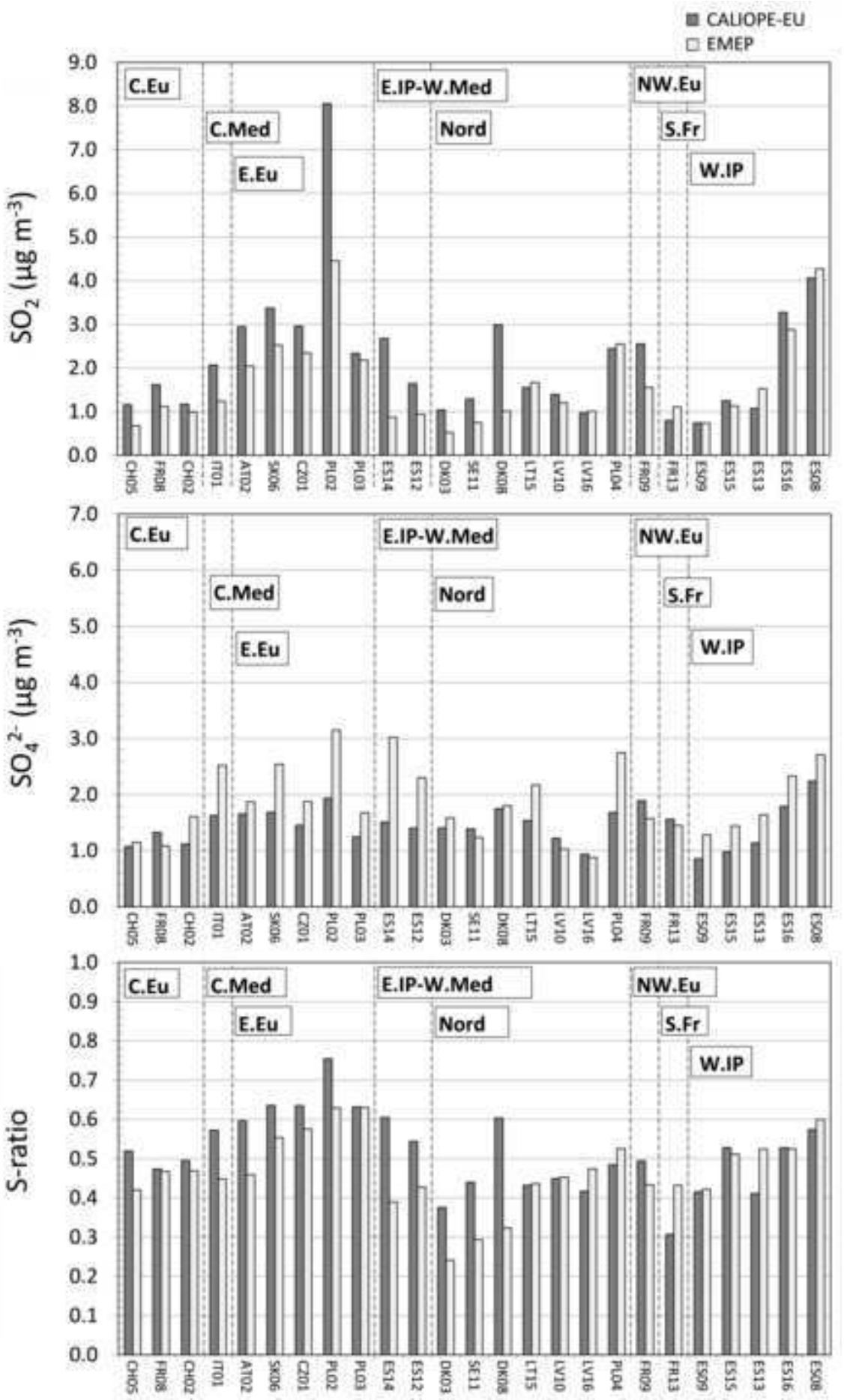

Figure8

Click here to download high resolution image

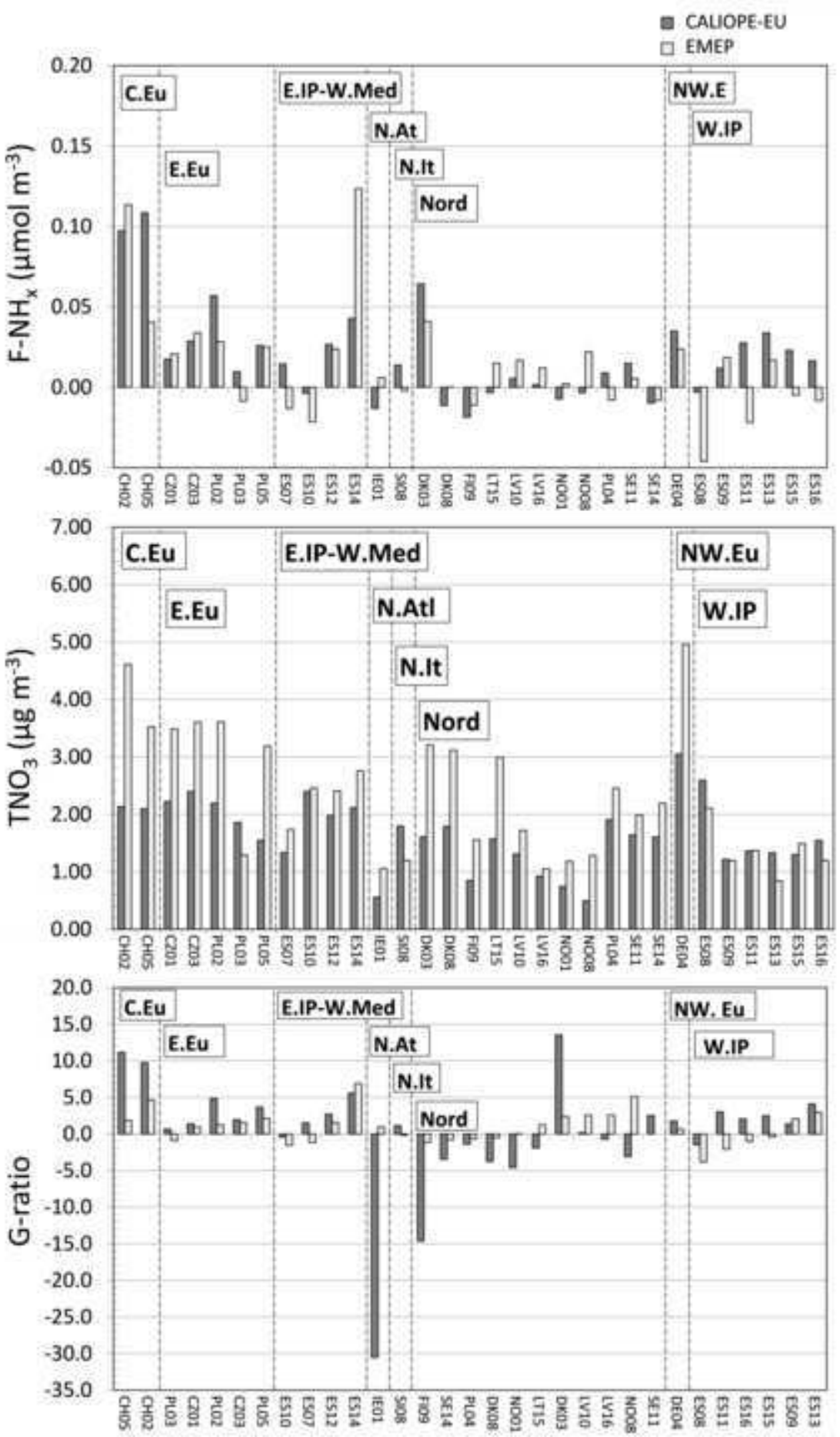

Table1

Click here to download Table: Table1.docx

Table 1. Total emission of SO_x, NO_x, NMVOC, PM2.5, PM coarse, CO and NH_3 for the year 2004 for anthropogenic activities in Europe sort by SNAP (Selected nomenclature air pollution) category.

SNAP	Description	SO_x	NO_x	NMVOC	PM2.5	PM coarse	CO	NH_3
1	Energy transformation	9323	3483	137	295	386	852	7
2	Small combustion sources	1161	1028	1163	825	314	10803	7
3	Industrial combustion	2096	2096	180	299	202	5499	6
4	Industrial process	734	385	1504	552	315	3643	106
5	Extraction of fossil fuels	0	0	0	0	0	0	0
6	Solvent and product use	0	0	4300	21	11	22	5
7	Road transport	314	6491	4355	361	95	26001	82
8	Non road transport	2868	6166	754	487	57	3115	2
9	Waste handling and disposal	25	41	159	97	15	1832	143
10	Agriculture	2	246	508	176	332	535	5823
	Total	16522	19937	13059	3113	1727	52303	6182

Table2

Click here to download Table: Table2.docx

Table 2. Coordinates, altitude and the chemical species measured of the 54 selected EMEP stations. The code is composed by 2-letter country code plus 2-digit station code. Zone is defined as follows: Western Iberian Peninsula (W.IP); Eastern Iberian Peninsula-Western Mediterranean (E.IP-W.Med), Central Mediterranean (C.Med), Eastern Mediterranean (E.Med), North of Italy (N. It.), Eastern Europe (E.Eu), Northwestern Europe (NW.Eu), Southern France (S.Fr.), Central Europe (C.Eu), Nordic (Nord), Central France (C.Fr) and North Atlantic (N.Atl).

	Station Name	Code	Zone	Lon.(º/N)	Lat.(º/E)	Alt.(m)	SO_4^{2-}	NO_3^-	NH_4^+	NH_3	HNO_3	TNH_3	TNO_3	SO_2
1	Anholt	DK08	Nord	56.717	11.517	40	x					x	x	x
2	Barcarrota	ES11	W.IP	38.476	-6.923	393	x	x				x	x	x
3	Birkenes	NO01	Nord	58.383	8.25	190	x	x	x	x	x	x	x	
4	Cabo de Creus	ES10	E.IP-W.Med	42.319	3.317	23	x	x				x	x	
5	Campisábalos	ES09	W.IP	41.281	-3.143	1360	x	x		x		x	x	x
6	Chopok	SK02	E.Eu	48.933	19.583	2008	x							
7	Deuselbach	DE04	NW.Eu	49.767	7.05	480	x					x	x	
8	Diabla Gora	PL05	E.Eu	54.15	22.067	157	x					x	x	
9	Donon	FR08	C.Eu	48.5	7.133	775	x							x
10	Els Torms	ES14	E.IP-W.Med	41.4	0.717	470	x	x				x	x	x
11	Eskdalemuir	GB02	NW.Eu	55.313	-3.204	243	x							
12	High Muffles	GB14	NW.Eu	54.334	-0.808	267	x							
13	Illmitz	AT02	E.Eu	47.767	16.767	117	x	x	x	x	x			x
14	Iraty	FR12	S.Fr	43.033	-1.083	1300	x							x
15	Iskrba	SI08	N.It	45.567	14.867	520	x					x	x	
16	Ispra	IT04	N.It	45.8	8.633	209	x	x	x					
17	Jarczew	PL02	E.Eu	51.817	21.983	180	x	x	x			x	x	x
18	Jungfraujoch	CH01	C.Eu	46.55	7.983	3573	x	x	x					
19	Kollumerwaard	NL09	NW.Eu	53.334	6.277	1		x	x					
20	Kosetice	CZ03	E.Eu	49.583	15.083	534	x					x	x	x
21	K-puszta	HU02	E.Eu	46.967	19.583	125	x	x	x	x	x			
22	La Tardière	FR15	C.Fr	46.65	0.75	746	x							
23	Le Casset	FR16	C.Eu	45	6.467	746	x							
24	Leba	PL04	Nord	54.75	17.533	2	x	x	x			x	x	x
25	Liesek	SK05	E.Eu	49.367	19.683	892	x	x			x			
26	Lough Navar	GB06	N.Atl	54.443	-7.87	126	x							
27	Melpitz	DE44	NW.Eu	52.53	12.93	86	x	x	x					
28	Montandon	FR14	C.Eu	47.183	6.5	746	x							
29	Montelibretti	IT01	C.Med	42.1	12.633	48	x	x	x	x	x			x
30	Morvan	FR10	C.Fr	47.267	4.083	620	x							
31	Niembro	ES08	W.IP	43.442	-4.85	134	x	x		x		x	x	x
32	O Savñao	ES16	W.IP	42.653	-7.705	506	x	x				x	x	x
33	Payerne	CH02	C.Eu	46.817	6.95	510	x					x	x	
34	Penausende	ES13	W.IP	41.283	-5.867	985	x	x				x	x	x
35	Peyrusse Vieille	FR13	S.Fr	43.375	0.104	236	x							x
36	Preila	LT15	Nord	55.35	21.067	5	x					x	x	x
37	Råö	SE14	Nord	57.4	11.917	5	x					x	x	
38	Revin	FR09	NW.Eu	49.9	4.633	390	x							x
39	Rigi	CH05	C.Eu	47.069	8.466	1030	x					x	x	x
40	Risco Llamo	ES15	W.IP	39.517	-4.35	1241	x	x				x	x	x
41	Rucava	LV10	Nord	56.217	21.217	5	x	x	x			x	x	x
42	Skreådalen	NO08	Nord	58.817	6.717	475	x	x	x	x	x	x	x	
43	Sniezka	PL03	E.Eu	50.733	15.733	1603	x	x	x			x	x	x
44	Starina	SK06	E.Eu	49.05	22.267	345	x	x			x			x
45	Svratouch	CZ01	E.Eu	49.733	16.033	737	x					x	x	x
46	Tange	DK03	Nord	56.35	9.6	13	x					x	x	x
47	Topolniky	SK07	E.Eu	47.96	17.861	113	x	x			x			
48	Utö	FI09	Nord	59.779	21.377	7	x		x			x	x	
49	Valentina Observatory	IE01	N.Atl	51.94	-10.244	11	x					x	x	
50	Vavihill	SE11	Nord	56.017	13.15	175	x					x	x	x
51	Víznar	ES07	E.IP-W.Med	37.233	-3.533	1265	x	x				x	x	
52	Yarner Wood	GB13	NW.Eu	50.596	-3.713	119	x							
53	Zarra	ES12	E.IP-W.Med	39.086	-1.102	885	x	x				x	x	x
54	Zoseni	LV16	Nord	57.133	25.917	183	x	x	x			x	x	x

Table 3. Bias correlation coefficient of the secondary inorganic aerosol and their gas precursors between each other for all the data points available for 2004. Mean and standard deviation (STD) of the bias are in $\mu g\ m^{-3}$.

	NH_3	NO_3^-	HNO_3	SO_2	SO_4^{2-}	NH_4^+
Mean	-1.36	-1.01	-0.97	0.50	-0.29	-0.45
STD	1.09	2.10	1.64	2.14	1.31	1.08
NH_3	1.00 (7/2562)	0.03 (7/2562)	0.55 (5/1830)	-0.03 (4/1464)	0.02 (7/2562)	0.07 (5/1830)
NO_3^-		1.00 (27/9882)	-0.16 (8/2928)	-0.06 (15/5490)	0.29 (26/9516)	0.75 (14/5124)
HNO_3			1.00 (8/2928)	-0.07 (3/1098)	0.04 (8/2928)	0.00 (5/1830)
SO_2				1.00 (31/11346)	0.01 (25/9150)	0.07 (7/2562)
SO_4^{2-}					1.00 (53/19398)	0.59 (14/5124)
NH_4^+						1.00 (15/5490)

[a]Value reported without parenthesis represents the correlation coefficient.

[b]The first and second values in parenthesis represent the number of stations and the number of data points respectively used to calculate the correlation coefficient.

Table4

Click here to download Table: Table4.docx

Table 4. List of published European model evaluation studies for secondary inorganic aerosol and their main characteristics to be compared with CALIOPE-EU evaluation results (this study).

Reference	Modeled Year[1]	Modeling System	Horizontal Resolution/layers	Chemical Mechanism[2]	Thermodynamic Inorganic Equilibrium[3]	Study number
This study	2004	CALIOPE	12 km x 12 km/15	CBM-IV	ISORROPIA	CALIOPE-EU04
Kim et al. (2011)	2001	POLYPHEMUS	0.5º x 0.5º/5	RACM	ISORROPIA	POLYPHEMUS1
Kim et al. (2011)	2001	POLYPHEMUS	0.5º x 0.5º/5	CB05	ISORROPIA	POLYPHEMUS2
Matthias (2008)	2001	CMAQ	54 km x 54 km/20	CBM-IV	ISORROPIA	CMAQ3
Stern et al. (2008)	2003	CHIMERE	0.25 º x 0.25 º/8	MELCHIOR	ISORROPIA	CHIMERE4
Stern et al. (2008)	2003	EURAD	125 km x 125 km/23	EuroRADM	RPMARES	EURAD4
Stern et al. (2008)	2003	LOTOS-EUROS	0.25º x 0.25º/4	CBM-IV	ISORROPIA	LOTOS-EUROS4
Stern et al. (2008)	2003	REM-CALGRID	0.25º x 0.25º/5	CBM-IV	ISORROPIA	REM-CALGRID4
Stern et al. (2008)	2003	LM-MUSCAT	0.25º x 0.25º/40	RACM	Hinneburg et al. (2007)	LM-MUSCAT4
Sartelet et al. (2007)	2001	POLYPHEMUS	0.5º x 0.5º/5	RACM	ISORROPIA	POLYPHEMUS5
Tarrasón et al. (2006)	2004	Unified EMEP	50 km x 50 km/20	EMEP	EQSAM	EMEP6
van Loon et al. (2004)	1999/2001	CHIMERE	0.5º x 0.5º/8	MELCHIOR	ISORROPIA	CHIMERE7
van Loon et al. (2004)	1999/2001	DEHM	50 km x 50 km/20	EMEP	EQSAM	DEHM7
van Loon et al. (2004)	1999/2001	Unified EMEP	50 km x 50 km/10	EMEP	EQSAM	EMEP7
van Loon et al. (2004)	1999/2001	MATCH	55 km x 55 km/10	EMEP	EQSAM	MATCH7
van Loon et al. (2004)	1999/2001	LOTOS	0.25º x 0.5º/3	CBM-IV	ISORROPIA	LOTOS7
van Loon et al. (2004)	1999/2001	CMAQ	36 km x 36 km/21	RADM2	ISORROPIA	CMAQ7
van Loon et al. (2004)	1999/2001	REM-CALGRID	0.25º x 0.5º	CBM-IV	ISORROPIA	REM-CALGRID7
Schaap et al. (2004)	1995	LOTOS	25 km x 25 km/3	CBM-IV	ISORROPIA	LOTOS8
Hass et al. (2003)	1995	DEHM	50 km x 50 km/10	CBM-IV	EQSAM	DEHM9
Hass et al. (2003)	1995	EURAD	27 km x 27 km/15	EuroRADM	RPMARES	EURAD9
Hass et al. (2003)	1995	EUROS	0.55º x 0.55º/4	CBM-IV	EQSAM	EUROS9
Hass et al. (2003)	1995	LOTOS	0.25º x 0.5º/3	CBM-IV	ISORROPIA	LOTOS9
Hass et al. (2003)	1995	MATCH	55 km x 55 km/10	EMEP	EQSAM	MATCH9
Hass et al. (2003)	1995	REM-CALGRID	0.25º x 0.5º	CBM-IV	ISORROPIA	REM-CALGRID9

[1]Evaluation studies are done over a full year. Evaluated period for Kim et al (2001) corresponds from 15 July to 15 August. Evaluated period for Stern et al. (2008) corresponds from 6 February to 30 March.

[2]CBM-IV, see Gery et al. (1989); CB05, see Yarwood et al. (2005); EMEP, see Simpson et al. (2003); EuroRADM, see Stockwell and Kley (1994); MELCHIOR, see Schmidt et al. (2001); RACM, see Stockwell et al. (1997); RADM2, see Stockwell et al. (1990).

[3]ISORROPIA, see Nenes et al. (1999); RPMARES, see Binkowski and Shankar (1995); EQSAM, see (Metzger et al., 2002).

Table5
Click here to download Table: Table5.docx

Table 5. Comparison of the statistics modeled mean/observed mean (Ratio), correlation coefficient (r), and root mean squared error (RMSE, μg m^{-3}) between CALIOPE and other European models[1,2] for secondary inorganic aerosol (SO_4^{2-}, NO_3^-, and NH_4^+) in daily basis.

Study Number	SO_4^{2-} daily average			NO_3^- daily average			NH_4^+ daily average		
	Ratio	r	RMSE	Ratio	r	RMSE	Ratio	r	RMSE
CALIOPE-EU04	0.82 (0.56,2.0)	0.49 (0.15,0.81)	1.30 (0.3,2.3)	0.50 (0.14,2.0)	0.58 (0.20,0.77)	2.30 (0.6,3.8)	0.67 (0.38,1.35)	0.62 (0.30,0.73)	1.20 (0.3,4.1)
POLYPHEMUS1	0.86			1.5			1.1		
POLYPHEMUS2	0.96			1.7			1.2		
CMAQ3	0.83 (0.54,1.36)	(0.21,0.72)		0.62 (0.39,1.0)	(0.30,0.80)		0.75 (0.53,0.94)	(0.30,0.75)	
CHIMERE4	0.69	0.48	3.4						
EURAD4	0.64	0.46	3.3						
LOTOS-EUROS4	0.57	0.47	3.7						
REM-CALGRID4	0.99	0.47	2.9						
LM-MUSCAT4	0.91	0.57	2.7						
POLYPHEMUS5	0.84	0.56	1.7	1.6	0.41	3.1	1.1	0.52	1.3
EMEP6	0.86	0.67		1.4	0.80		1.2	0.82	
CHIMERE7	0.67/0.72	0.49/0.53	2.5/2.07	0.94/0.80	0.44/0.46	2.74/2.73	1.11/1.01	0.41/0.56	1.27/1.38
DEHM7	0.93/0.85	0.57/0.55	2.36/1.77	1.80/1.63	0.34/0.25	3.02/2.53	1.10/0.79	0.51/0.49	0.98/0.83
EMEP7	0.91/0.88	0.57/0.58	2.1/1.84	1.63/1.04	0.50/0.34	3.51/2.08	1.26/1.00	0.51/0.47	1.22/0.86
MATCH7	1.0/1.17	0.56/0.62	2.1/1.86	0.88/0.83	0.47/0.40	1.74/1.59	1.01/1.62	0.53/0.55	0.94/2.09
LOTOS7	1.03/1.3	0.37/0.50	2.9/2.89	0.79/0.95	0.26/0.17	2.19/1.94	1.21/1.01	0.37/0.44	1.21/1.10
CMAQ7	1.22/-	0.46/-	2.67/-	2.65/-	0.47/-	1.74/-	-/-	-/-	-/-
REM-CALGRID7	0.91/0.93	0.51/0.53	2.36/2.03	1.15/0.74	0.42/0.35	2.43/1.92	1.33/1.23	0.45/0.45	1.24/0.99
LOTOS8	0.92	0.60	2.60	1.10	0.58	3.57	1.08	0.62	1.54
DEHM9	1.11	0.37	5.89	1.07	0.32	4.12	0.94	0.39	2.43
EURAD9	1.52	0.52	4.25	2.04	0.61	6.14	1.87	0.50	2.90
EUROS9	0.98	0.47	4.39	2.13	0.30	6.39	-	-	-
LOTOS9	0.91	0.54	2.76	1.59	0.49	4.07	1.23	0.51	1.57
MATCH9	0.84	0.65	2.49	0.78	0.50	2.55	0.55	0.61	1.46
REM-CALGRID9	0.81	0.50	2.78	1.07	0.53	3.10	1.07	0.43	1.63

[1]Value reported without parenthesis represents yearly averages in the entire domain. The first and second values in parenthesis represent the minimum and maximum value respectively obtained among all stations in the entire domain. [2]Values reported with a slash correspond to two different years studied: the number before the slash corresponds to the year 1999; the number after the slash correspond to the year 2001.

Table6

Click here to download Table: Table6.docx

Table 6. Comparison of the statistics modeled mean/observed mean (Ratio), correlation coefficient (r), and root mean squared error (RMSE, μg m^{-3}) between CALIOPE and other European models[1,2] for total nitrate (TNO_3 = HNO_3+NO_3^-), total ammonia (TNH_3=NH_3+NH_4^+) and gas-phase aerosol precursors (HNO_3 and NH_3) in daily basis. Note that the other gas-phase aerosol precursors, SO_2 and NO_2 have been compared with other European studies in Pay et al. (2010).

Study Number	HNO_3 daily average			TNO_3 daily average			NH_3 daily average			TNH_3 daily average		
	Ratio	r	RMSE	Ratio	r	RMSE	Ratio	r	RMSE	Ratio	r	RMSE
CALIOPE-EU04	1.00 (0.35,4.0)	0.41 (-0.11,0.78)	1.1 (0.4,3.5)	0.77 (0.45,1.2)	0.50 (0.14,0.70)	2.1 (0.9,3.6)	0.71 (0.1,1.0)	0.56 (0.10,0.40)	1.1 (0.3,1.3)	0.94 (0.62,2)	0.50 (0.10,0.72)	1.8 (0.4,3.3)
CHIMERE4				0.70	0.47	4.4				1.1	0.49	1.9
EURAD4				2.90	0.46	19.4				3.0	0.45	8.3
LOTOS-EUROS4				0.94	0.67	3.1				1.0	0.58	1.6
REM-CALGRID4				0.87	0.56	3.5				1.4	0.57	2.1
LM-MUSCAT4				0.44	0.42	5.8				1.6	0.56	3.5
POLYPHEMUS5	1.85	0.26	1.4				0.85	0.29	5.4			
EMEP6	0.73	0.38		1.23	0.87					1.26	0.63	
CHIMERE7				0.90/0.83	0.39/0.37	3.02/2.82				1.18/1.05	0.35/0.43	2.98/1.74
DEHM7				1.68/1.73	0.42/0.31	3.03/3.02				0.86/0.79	0.46/0.45	1.85/1.14
EMEP7				1.40/1.16	0.51/0.36	2.62/2.42				1.05/1.00	0.42/0.40	1.95/1.28
MATCH7				0.85/0.95	0.52/0.41	1.88/1.91				0.71/1.62	0.48/0.42	1.82/2.17
LOTOS7				0.72/0.70	0.23/0.20	2.31/2.27				1.12/1.01	0.27/0.29	2.25/1.49
CMAQ7				1.82/-	0.52/-	1.88/-				-/-	-/-	-/-
REM-CALGRID7				1.10/0.86	0.39/0.31	2.26/3.02				1.35/1.23	0.27/0.30	2.39/1.49
LOTOS8				0.81	0.52	2.31				0.88	0.58	1.50
DEHM9				1.09	0.45	2.75	0.38	0.27	7.38	0.79	0.47	3.69
EURAD9				1.85	0.50	3.72	0.56	0.15	5.88	1.24	0.54	3.40
EUROS9				2.49	0.41	5.17	-	-	-	-	-	-
LOTOS9				1.67	0.44	2.82	0.18	0.05	7.50	0.58	0.46	2.77
MATCH9				0.94	0.52	1.94	0.64	0.33	5.59	0.84	0.57	2.54
REM-CALGRID9				1.20	0.38	2.13	0.58	0.09	6.10	0.91	0.26	3.09

[1]Value reported without parenthesis represents yearly averages in the entire domain. The first and second values in parenthesis represent the minimum and maximum value respectively obtained among all stations in the entire domain. [2]Values reported with a slash correspond to two different years studied: the number before the slash corresponds to the year 1999; the number after the slash correspond to the year 2001.